J. Fluid Mech. (1995), *vol.* 291, *pp.* 1–32
Copyright © 1995 Cambridge University Press

The motion of a rising disk in a rotating axially bounded fluid for large Taylor number

By MARIUS UNGARISH† AND DMITRY VEDENSKY
Department of Computer Science, Technion, Haifa 32000, Israel

(Received 7 February 1994 and in revised form 8 November 1994)

The motion of a disk rising steadily along the axis in a rotating fluid between two infinite plates is considered. In the limit of zero Rossby number and with the disk in the middle position, the boundary value problem based on the linear, viscous equations of motion is reduced to a system of dual-integral equations which renders 'exact' solutions for arbitrary values of the Taylor number, Ta, and disk-to-wall distance, H (scaled by the radius of the disk). The investigation is focused on the drag and on the flow field when Ta is large (but finite) for various H. Comparisons with previous asymptotic results for 'short' and 'long' containers, and with the preceding unbounded-configuration 'exact' solution, provide both confirmation and novel insights.

In particular, it is shown that the 'free' Taylor column on the particle appears for $H > 0.08\,Ta$ and attains its fully developed features when $H > 0.25\,Ta$ (approximately). The present drag calculations improve the compatibility of the linear theory with Maxworthy's (1968) experiments in short containers, but for the long container the claimed discrepancy with experiments remains unexplained.

1. Introduction

The present study is an extension of the investigation by Vedensky & Ungarish (1994, hereafter referred to as VU) concerning the parallel-to-axis ('vertical') motion of a disk in an *unbounded* rotating fluid. The obvious deficiency of that analysis is the omission of the practically unavoidable influence of the boundaries, especially of the 'horizontal' walls. When the Taylor number, Ta, is large these walls evidently modify or suppress the tendency of the flow field to form the long 'free' Taylor columns detected in the unbounded configuration. The present work incorporates the parallel-to-disk boundaries in the 'exact' solution of the full linear-theory equations of motion and focuses on the flow field and drag features for $Ta \gg 1$.

The basic configuration is shown in figure 1: the disk, of radius a^*, is moving with constant velocity V^* toward the upper boundary; we consider exactly the midway instance, i.e. both walls are at distance H^* from the disk. The walls and the far-from-the-disk fluid rotate with constant Ω^* around the axis of symmetry. Asterisks denote dimensional variables. We use a cylindrical r, θ, z coordinate system rotating with Ω^* around z in which $\boldsymbol{v}^* = \{u^*, v^*, w^*\}$ is the velocity vector. Hereafter t^* is time, ρ^* and ν^* are the density and kinematic viscosity of the fluid, P^* is the reduced pressure and D^* the drag force on the particle.

† To whom correspondence should be addressed.

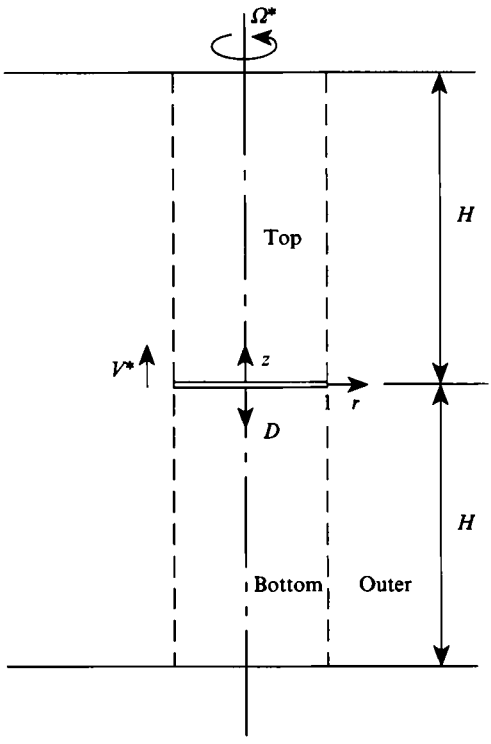

FIGURE 1. Configuration.

The analysis is conveniently performed in dimensionless form by employing the following scalings:

$$\{\boldsymbol{r}^*, t^*, \boldsymbol{v}^*, P^*, D^*\} = \left\{a^*\boldsymbol{r}, \frac{a^*}{V^*}t, V^*\boldsymbol{v}, \frac{V^*\nu^*\rho^*}{a^*}P, V^*\nu^*\rho^*a^*D\right\}. \tag{1}$$

Now the equations of conservation of mass and momentum read

$$\boldsymbol{\nabla}\cdot\boldsymbol{v} = 0, \tag{2}$$

$$(Ro\,Ta)\frac{\partial \boldsymbol{v}}{\partial t} + (Ro\,Ta)\,\boldsymbol{v}\cdot\boldsymbol{\nabla}\boldsymbol{v} + 2Ta(\hat{\boldsymbol{z}}\times\boldsymbol{v}) = -\boldsymbol{\nabla}P - \boldsymbol{\nabla}\times\boldsymbol{\nabla}\times\boldsymbol{v}. \tag{3}$$

The independent dimensionless parameters governing the flow field generated by the motion of the particle are

$$Ta = \frac{a^{*2}\Omega^*}{\nu^*}, \quad Ro = \frac{V^*}{\Omega^* a^*}, \quad H = \frac{H^*}{a^*}. \tag{4}$$

The Taylor number, Ta, expresses the typical ratio of the Coriolis to the viscous forces in the fluid (Ta is actually the inverse of the Ekman number of the particle). The Rossby number, Ro, a ratio of the convective to the Coriolis accelerations, estimates the relative importance of nonlinear terms.

Setting $Ro = 0$ in (3) yields the important linear steady formulation, which we adopt here.

The boundary conditions are no penetration and no slip on the particle and on the walls $z = \pm H$. In the unbounded configuration the present conditions at $z = \pm H$ are replaced by unperturbed solid-body rotation at $z^2 + r^2 \to \infty$. It is expected that the present analysis for finite H recovers the unbounded case when $H \to \infty$. In general, a torque-free rising disk rotates slightly, but this rotation vanishes in the symmetric configuration under consideration.

To be specific, in the present study we shall consider $Ta \gg 1$ flows and configurations with $H > 10/Ta^{1/2}$ (i.e. there is some 'core' outside the developed Ekman layers whose typical thickness is $3/Ta^{1/2}$ each).

For the relevant configuration, two different ranges of H have received theoretical consideration in the literature: $H \ll Ta^{1/2}$, roughly referred to as a short container, by Moore & Saffman (1968, 1969); $H \gg Ta^{1/2}$, hereafter referred to as a long container, by Hocking, Moore & Walton (1978). In the first range analytical progress was attained by decomposing the flow in the geostrophic cores, Ekman ('horizontal') boundary layers and Stewartson ('vertical') shear layers. It was shown that the flow field is dominated by the Ekman layers, the swirl velocities in the up- and downstream regions are $O(Ta^{1/2})$ and the drag is $O(Ta^{3/2})$. The drag force on a disk is about 22% higher than on a sphere. In the analysis of the second range the Ekman layer influence, expected to be minor, was neglected. It turned out that, like in the unbounded configuration, the swirl velocities in the up- and downstream regions are $O(1)$ and the drag is $O(Ta)$; the drag forces on a disk and a sphere are the same.

The above-mentioned studies leave open some important questions. First, the range of applicability is established only asymptotically with respect to large Ta. It is not clear in practice which particular values of Ta can be considered sufficiently large and what error shows up for a given set of Ta, H. Moreover, the solutions certainly do not span the whole range of H and do not give indications of the behaviour in the intermediate (moderately long container) domain. In this intermediate range the swirl velocity varies from $O(Ta^{1/2})$ to $O(1)$ as H varies from the lower to the upper values.

Secondly, the experimental verifications of the drag by Maxworthy (for spherical particles) revealed discrepancies with the analytical results that have not been satisfactorily explained.

Thirdly, the analysis of the flow field in the first range of H was closed by an *ad hoc* assumption of Kutta–Joukowsky type; therefore independent verifications of the results are desirable. In particular, it was predicted on this basis that the meridional velocities in the inner Stewartson layer are higher than necessary for the $O(1)$ volume flux transport; actually, an $O(Ta^{1/12})$ recirculation was predicted. This peculiar feature has not been verified.

Fourth, in the unbounded configuration when $Ta > 37$ a distinct region ('bubble') of recirculation appears near the body; this becomes the main part of the 'free' Taylor column for large Ta, as reported by VU for a disk and by Tanzosh & Stone (1994) for a sphere. The expectedly critical influence of H on this flow-field feature is worthy of investigation.

The present study endeavours to close the above-mentioned gaps in knowledge via an 'exact' solution by the dual-integral equations method. Essentially, the approach is correct for arbitrary values of Ta and H. However, the final computational procedure is developed for $H\,Ta^{1/2} > 10$ and the computations appear to be reliable up to $Ta \approx 30000$.

The outline of this paper is as follows. In §2 the governing equations of motion are reformulated as dual integral equations, from which the formal solution of the problem is obtained. Analysis of the drag and the flow field for small and moderate H is

performed in §3. In §4 attention is focused on the large-H case. Concluding remarks are presented in §5.

2. Formal solution

2.1. *Governing equations*

In view of the axial symmetry, the scalar form of the governing equations (2) and (3) is

$$-2Tav = -\frac{\partial P}{\partial r} + \left(\frac{\partial^2 u}{\partial r^2} + \frac{\partial u}{r\,\partial r} - \frac{u}{r^2} + \frac{\partial^2 u}{\partial z^2}\right), \tag{5}$$

$$2Tau = \left(\frac{\partial^2 v}{\partial r^2} + \frac{\partial v}{r\,\partial r} - \frac{v}{r^2} + \frac{\partial^2 v}{\partial z^2}\right), \tag{6}$$

$$0 = -\frac{\partial P}{\partial z} + \left(\frac{\partial^2 w}{\partial r^2} + \frac{\partial w}{r\,\partial r} + \frac{\partial^2 w}{\partial z^2}\right), \tag{7}$$

$$\frac{\partial (ru)}{r\,\partial r} + \frac{\partial w}{\partial z} = 0. \tag{8}$$

Here r and z are the radius and axial coordinate in a cylindrical frame attached to the centre of the disk and rotating with the walls.

To close the boundary value problem the conditions on the disk and the walls should be specified. Since the equations do not contain convection terms and the domain is fore–aft symmetric, the torque-free disk will not rotate relative to the fluid. So

$$u = v = w = 0 \quad \text{at} \quad 0 \leqslant r \leqslant 1, \quad z = 0; \tag{9}$$

$$u = v = 0; \quad w = -1 \quad \text{at} \quad z = H, -H. \tag{10}$$

2.2. *The Hankel-transform formulation*

Since the governing equations are the same as for the unbounded case (see VU, §2), the general solution, which was determined on the basis of the Hankel transform and determining of the eigenvalues of the system, is already available. The only difference is that now, because the domain is bounded in z, we cannot discard the terms which increase exponentially with the distance from the disk (see (33) and (34) in VU).

Let p be the variable of the Hankel transform (not to be confused with the pressure P). The flow field can be expressed in terms of the known λ_1, λ_2 and λ_3 (the solutions to the characteristic equation $\lambda^3 + (4Ta^2/p^4)(\lambda + 1) = 0$, see Appendix A), and the unknown functions of p α_1, α_2, β_1, β_2, γ_1 and γ_2, which should be determined by the boundary conditions.

The solution for the upstream half-space ($z \geqslant 0$) reads

$$\begin{aligned} v(r,z) = \int_0^\infty pJ_1(rp)\,[&\alpha_1 \sinh(p(1+\lambda_1)^{1/2} z) + \alpha_2 \cosh(p(1+\lambda_1)^{1/2} z) \\ &+ \beta_1 \sinh(p(1+\lambda_2)^{1/2} z) + \beta_2 \cosh(p(1+\lambda_2)^{1/2} z) \\ &+ \gamma_1 \sinh(p(1+\lambda_3)^{1/2} z) + \gamma_2 \cosh(p(1+\lambda_3)^{1/2} z)]\,\mathrm{d}p, \end{aligned} \tag{11}$$

$$u(r,z) = \frac{1}{2Ta}\int_0^\infty p^3 J_1(rp)\,[\lambda_1\alpha_1\sinh(p(1+\lambda_1)^{1/2}z) + \lambda_1\alpha_2\cosh(p(1+\lambda_1)^{1/2}z) + \lambda_2\beta_1\sinh(p(1+\lambda_2)^{1/2}z) + \lambda_2\beta_2\cosh(p(1+\lambda_2)^{1/2}z) + \lambda_3\gamma_1\sinh(p(1+\lambda_3)^{1/2}z) + \lambda_3\gamma_2\cosh(p(1+\lambda_3)^{1/2}z)]\,dp, \tag{12}$$

$$w(r,z) = -1 - \frac{1}{2Ta}\int_0^\infty p^3 J_0(rp)\left[\alpha_1\frac{\lambda_1}{(1+\lambda_1)^{1/2}}\cosh(p(1+\lambda_1)^{1/2}z) + \alpha_2\frac{\lambda_1}{(1+\lambda_1)^{1/2}}\sinh(p(1+\lambda_1)^{1/2}z) + \beta_1\frac{\lambda_2}{(1+\lambda_2)^{1/2}}\cosh(p(1+\lambda_2)^{1/2}z) + \beta_2\frac{\lambda_2}{(1+\lambda_2)^{1/2}}\sinh(p(1+\lambda_2)^{1/2}z) + \gamma_1\frac{\lambda_3}{(1+\lambda_3)^{1/2}}\cosh(p(1+\lambda_3)^{1/2}z) + \gamma_2\frac{\lambda_3}{(1+\lambda_3)^{1/2}}\sinh(p(1+\lambda_3)^{1/2}z)\right]dp. \tag{13}$$

For the stream function, $\psi(r,z)$, prescribing $\psi = 0$ on the axis and on the disk, on account of (13) one obtains

$$\psi(r,z) = \int_0^r r'w(r',z)\,dr' = -\frac{r^2}{2} - \frac{1}{2Ta}\int_0^\infty rp^2 J_1(rp)\left[\alpha_1\frac{\lambda_1}{(1+\lambda_1)^{1/2}}\cosh(p(1+\lambda_1)^{1/2}z) + \alpha_2\frac{\lambda_1}{(1+\lambda_1)^{1/2}}\sinh(p(1+\lambda_1)^{1/2}z) + \beta_1\frac{\lambda_2}{(1+\lambda_2)^{1/2}}\cosh(p(1+\lambda_2)^{1/2}z) + \beta_2\frac{\lambda_2}{(1+\lambda_2)^{1/2}}\sinh(p(1+\lambda_2)^{1/2}z) + \gamma_1\frac{\lambda_3}{(1+\lambda_3)^{1/2}}\cosh(p(1+\lambda_3)^{1/2}z) + \gamma_2\frac{\lambda_3}{(1+\lambda_3)^{1/2}}\sinh(p(1+\lambda_3)^{1/2}z)\right]dp. \tag{14}$$

The pressure in the plane of the disk, in view of (5), (11) and (12) and the prescription $P = 0$ at $r^2+z^2 \to \infty$, reads

$$P(r, z = 0^+) = -\frac{1}{2Ta}\int_0^\infty p^4 J_0(rp)\,[\alpha_2\lambda_1^2 + \beta_2\lambda_2^2 + \gamma_2\lambda_3^2]\,dp. \tag{15}$$

The form of the governing equations and the symmetry of the configuration suggest symmetry relationships about the plane of the disk in the flow field considered, i.e.

$$u(r,z) = -u(r,-z), \quad v(r,z) = -v(r,-z), \tag{16a, b}$$

$$w(r,z) = w(r,-z), \quad P(r,z) = -P(r,-z). \tag{16c, d}$$

Essentially these conditions are not independent; (16*c*) immediately follows from (16*a*) and (8), and (16*d*) results from (16*a*), (16*b*) and (5). Consequently, it is sufficient to develop the solution for the half-space $z \geqslant 0$.

To evaluate the entire flow field the six unknown functions of p α_1, α_2, β_1, β_2, γ_1, and γ_2 are to be determined; Ta and H enter as parameters. To find these functions we apply symmetry and boundary conditions on the general solution. This we perform in two stages: (*a*) we express in terms of α_2 the other five functions, as shown in §2.3; (*b*) we obtain and solve a dual-integral equation for α_2, as detailed in §2.4.

2.3. *Reducing the number of functions sought*

We notice that the symmetry condition (16) actually implies that

$$u(r, z = 0) = v(r, z = 0) = 0 \tag{17}$$

for any r. The fulfillment of (17) for any r imposes, via (11) and (12),

$$\alpha_2 + \beta_2 + \gamma_2 = 0, \tag{18}$$

$$\lambda_1 \alpha_2 + \lambda_2 \beta_2 + \lambda_3 \gamma_2 = 0. \tag{19}$$

Solving for β_2 and γ_2 in terms of α_2,

$$\beta_2 = \alpha_2 \frac{\lambda_1 - \lambda_3}{\lambda_3 - \lambda_2}, \quad \gamma_2 = \alpha_2 \frac{\lambda_2 - \lambda_1}{\lambda_3 - \lambda_2}, \tag{20}$$

reduces the number of unknown functions to four. Next, the application of the boundary conditions (10) on the wall $z = H$ results, after dividing by α_2 through (20), in the linear system of three equations with three variables α_1/α_2, β_1/α_2 and γ_1/α_2.

$$\frac{\alpha_1}{\alpha_2}\sinh(p(1+\lambda_1)^{1/2}H) + \frac{\beta_1}{\alpha_2}\sinh(p(1+\lambda_2)^{1/2}H) + \frac{\gamma_1}{\alpha_2}\sinh(p(1+\lambda_3)^{1/2}H)$$

$$= -\left[\cosh(p(1+\lambda_1)^{1/2}H) + \frac{\beta_2}{\alpha_2}\cosh(p(1+\lambda_2)^{1/2}H) + \frac{\gamma_2}{\alpha_2}\cosh(p(1+\lambda_3)^{1/2}H)\right]; \tag{21a}$$

$$\lambda_1\frac{\alpha_1}{\alpha_2}\sinh(p(1+\lambda_1)^{1/2}H) + \lambda_2\frac{\beta_1}{\alpha_2}\sinh(p(1+\lambda_2)^{1/2}H) + \lambda_3\frac{\gamma_1}{\alpha_2}\sinh(p(1+\lambda_3)^{1/2}H)$$

$$= -\left[\lambda_1\cosh(p(1+\lambda_1)^{1/2}H) + \lambda_2\frac{\beta_2}{\alpha_2}\cosh(p(1+\lambda_2)^{1/2}H) + \lambda_3\frac{\gamma_2}{\alpha_2}\cosh(p(1+\lambda_3)^{1/2}H)\right]; \tag{21b}$$

$$\frac{\lambda_1}{(1+\lambda_1)^{1/2}}\frac{\alpha_1}{\alpha_2}\cosh(p(1+\lambda_1)^{1/2}H) + \frac{\lambda_2}{(1+\lambda_2)^{1/2}}\frac{\beta_1}{\alpha_2}\cosh(p(1+\lambda_2)^{1/2}H)$$

$$+\frac{\lambda_3}{(1+\lambda_3)^{1/2}}\frac{\gamma_1}{\alpha_2}\cosh(p(1+\lambda_3)^{1/2}H) = -\left[\frac{\lambda_1}{(1+\lambda_1)^{1/2}}\sinh(p(1+\lambda_1)^{1/2}H)\right.$$

$$\left.+\frac{\lambda_2}{(1+\lambda_2)^{1/2}}\frac{\beta_2}{\alpha_2}\sinh(p(1+\lambda_2)^{1/2}H) + \frac{\lambda_3}{(1+\lambda_3)^{1/2}}\frac{\gamma_2}{\alpha_2}\sinh(p(1+\lambda_3)^{1/2}H)\right]. \tag{21c}$$

Formally, from the (21) exact expressions for α_1/α_2, β_1/α_2 and γ_1/α_2 as functions of p with Ta and H as parameters, can be obtained. However, in order to avoid the loss of significance and 'overflow' errors which accompany the direct solution of (21) when $HTa^{1/2} \gg 1$, an asymptotic approach was used. The relevant analysis, details of which

may be obtained from the authors or JFM Editorial Office (see also Appendix A), reveals

(*a*) For arbitrary $p \geqslant 0$

$$\frac{\beta_1}{\alpha_2} = -\frac{\beta_2}{\alpha_2}(1+O(\mathrm{e}^{-H\,Ta^{1/2}})), \quad \frac{\gamma_1}{\alpha_2} = -\frac{\gamma_2}{\alpha_2}(1+O(\mathrm{e}^{-H\,Ta^{1/2}})), \tag{22}$$

$$\frac{\alpha_1}{\alpha_2} =$$

$$-\frac{(1+\lambda_2)^{1/2}\left(1-\dfrac{\lambda_1}{\lambda_2}\right)-(1+\lambda_3)^{1/2}\left(1-\dfrac{\lambda_1}{\lambda_3}\right)+\dfrac{\lambda_1}{(1+\lambda_1)^{1/2}}(\lambda_3-\lambda_2)\dfrac{(1+\lambda_2)^{1/2}(1+\lambda_3)^{1/2}}{\lambda_2\lambda_3}t_1}{\left[(1+\lambda_2)^{1/2}\left(1-\dfrac{\lambda_1}{\lambda_2}\right)-(1+\lambda_3)^{1/2}\left(1-\dfrac{\lambda_1}{\lambda_3}\right)\right]t_1+\dfrac{\lambda_1}{(1+\lambda_1)^{1/2}}(\lambda_3-\lambda_2)\dfrac{(1+\lambda_2)^{1/2}(1+\lambda_3)^{1/2}}{\lambda_3\lambda_2}}$$

$$\times(1+O(\mathrm{e}^{-H\,Ta^{1/2}})), \tag{23}$$

where $t_1 = \tanh((1+\lambda_1)^{1/2}pH)$.

(*b*) For $p \to \infty$

$$\frac{\alpha_1}{\alpha_2} = -1+O(\mathrm{e}^{-pH}), \quad \frac{\beta_1}{\alpha_2} = -\frac{\beta_2}{\alpha_2}(1+O(\mathrm{e}^{-pH})), \quad \frac{\gamma_1}{\alpha_2} = -\frac{\gamma_2}{\alpha_2}(1+O(\mathrm{e}^{-pH})). \tag{24}$$

Hereafter we use the approximations (22)–(24), together with (20), as a substitute for the direct solution of (21), with tight control on the error propagation. Essentially, system (22)–(24) is indeed a simple, see (20), and an excellent approximation: the error is beyond the fourth significant decimal digit when $H\,Ta^{1/2} > 10$ and is of the order of the round-off unit of a 16 decimal digits (double-precision) computation when $H\,Ta^{1/2} \geqslant 40$. In the present work we performed calculations with 16 decimal digits, and considered configurations with $H\,Ta^{1/2} \geqslant 40$.† We expect that the drag and flow field so computed will reproduce, within machine accuracy, the results tentatively attainable with the exact solution of (21).

2.4. *Dual-integral equations solution*

Now the main task is the determination of the function α_2. To this end a system of dual-integral equations is formulated. The physical sense of these equations is the same as for the unbounded case. The first equation expresses the no-penetration requirement on the disk surface, which, by virtue of (13) for $z = 0$, reads

$$\frac{1}{2Ta}\int_0^\infty p^3 J_0(rp)\left[\frac{\alpha_1}{\alpha_2}\frac{\lambda_1}{(1+\lambda_1)^{1/2}}+\frac{\beta_1}{\alpha_2}\frac{\lambda_2}{(1+\lambda_2)^{1/2}}+\frac{\gamma_1}{\alpha_2}\frac{\lambda_3}{(1+\lambda_3)^{1/2}}\right]$$

$$\times\alpha_2(p, Ta, H)\,\mathrm{d}p = -1 \quad \text{for} \quad 0 \leqslant r < 1. \tag{25}$$

The complementary equation is based on the pressure continuity at $z = 0$, $r > 1$, which, in view of (16*d*) reads simply

$$P(r, z=0) = 0 \quad \text{for} \quad r > 1. \tag{26}$$

† With few marginal exceptions: (*a*) In figure 2 $H\,Ta^{1/2}$ is below 40 but still above 20 for some points with $H < 1$. (*b*) $H\,Ta^{1/2} \approx 32$ in the first line of table 1.

On account of (15) and (20) the last equation yields

$$\int_0^\infty p^4 J_0(rp)\left[\lambda_1^2+\lambda_2^2\frac{\lambda_1-\lambda_3}{\lambda_3-\lambda_2}+\lambda_3^2\frac{\lambda_2-\lambda_1}{\lambda_3-\lambda_2}\right]\alpha_2(p, Ta, H)\,\mathrm{d}p = 0 \quad \text{for} \quad r > 1. \tag{27}$$

On account of (20) and (22) the integrands in (25) and (27) are the products of the 'unknown' function $\alpha_2(p, Ta, H)$ and computable functions. Thus, as for the unbounded case, the solution $\alpha_2(p)$, with Ta and H as parameters, can be sought by Tranter's method.

In general, consider the dual-integral equations

$$\int_0^\infty \tilde{G}(p) f(p) J_0(rp)\,\mathrm{d}p = A, \quad 0 < r < 1, \tag{28}$$

$$\int_0^\infty f(p) J_0(rp)\,\mathrm{d}p = 0, \quad r > 1, \tag{29}$$

where $f(p)$ is the unknown function, $\tilde{G}(p)$ is a prescribed function and A a given parameter. Tranter showed that the system (28)–(29) is satisfied by

$$f(p) = p^{1-k}\sum_{m=0}^{\infty} a_m J_{2m+k}(p), \tag{30}$$

where the coefficients a_m are prescribed by the linear system

$$a_0 + \sum_{m=0}^{\infty} L_{0,m}\, a_m = \frac{2^{1-k}}{\Gamma(k)}A, \tag{31}$$

$$a_n + \sum_{m=0}^{\infty} L_{n,m}\, a_m = 0 \quad \text{for} \quad n \geqslant 1, \tag{32}$$

where

$$L_{n,m} = (4n+2k)\int_0^\infty [p^{2-2k}\tilde{G}(p) - 1]\, p^{-1} J_{2m+k}(p) J_{2n+k}(p)\,\mathrm{d}p. \tag{33}$$

Comparing our problem, which is described by the dual-integral equations (25) and (27), with (28)–(29) it is seen that by identifying

$$A = 2, \quad \tilde{G}(p) = -\frac{2}{p}\frac{\theta(p)}{\eta(p)}, \quad f(p) = -\frac{p^4 \eta(p)\,\alpha_2(p)}{2Ta}, \tag{34}$$

where

$$\theta(p) = \frac{\alpha_1}{\alpha_2}\frac{\lambda_1}{(1+\lambda_1)^{1/2}} + \frac{\beta_1}{\alpha_2}\frac{\lambda_2}{(1+\lambda_2)^{1/2}} + \frac{\gamma_1}{\alpha_2}\frac{\lambda_3}{(1+\lambda_3)^{1/2}}, \tag{35}$$

$$\eta(p) = \frac{\lambda_1^2(\lambda_3-\lambda_2) + \lambda_2^2(\lambda_1-\lambda_3) + \lambda_3^2(\lambda_2-\lambda_1)}{\lambda_3-\lambda_2}, \tag{36}$$

the exact form of equations (28)–(29) is recovered.

The function $\eta(p)$ has exactly the same form as its counterpart in the unbounded configuration. For the preceding function, in view of (20) and (22) we obtain, within $O(\mathrm{e}^{-Ta^{1/2}H})$ accuracy, for any $p \geqslant 0$,

$$\theta(p) = \frac{\alpha_1}{\alpha_2}\frac{\lambda_1}{(1+\lambda_1)^{1/2}} + \frac{\lambda_2}{(1+\lambda_2)^{1/2}}\frac{\lambda_1-\lambda_3}{\lambda_3-\lambda_2} + \frac{\lambda_3}{(1+\lambda_3)^{1/2}}\frac{\lambda_2-\lambda_1}{\lambda_3-\lambda_2}. \tag{37}$$

However, in view of (24), (35) yields

$$\theta(p) = \frac{\lambda_1}{(1+\lambda_1)^{1/2}} + \frac{\lambda_2}{(1+\lambda_2)^{1/2}}\frac{\lambda_1-\lambda_3}{\lambda_3-\lambda_2} + \frac{\lambda_3}{(1+\lambda_3)^{1/2}}\frac{\lambda_2-\lambda_1}{\lambda_3-\lambda_2} + O(\mathrm{e}^{-pH}) \quad \text{for} \quad p \to \infty, \tag{38}$$

which coincides with $\theta(p)$ of the unbounded case.

Thus, formally at least, for the present $\tilde{G}(p)$ and A, the unknown function $f(p)$ can be determined from the dual-integral equations by Tranter's method, and subsequently via (34) the function α_2 can be obtained. (For practical solutions the convergence and stability of (32)–(33) are essential, as discussed in the next subsection.) Next, application of (20) gives β_2 and γ_2, and (21) determines $\alpha_1, \beta_1, \gamma_1$. Finally, through (11)–(13) the physical variables can be evaluated.

However, direct calculation by means of (11)–(13) leads again, in view of (22)–(24), to loss of significance and 'overflow' errors which can be avoided by means of reformulation. For example, we rewrite (11) as follows:

$$v = \int_0^\infty pJ_1(rp)\frac{\alpha_2}{2}V_1(p,z)\,\mathrm{d}p, \tag{39}$$

where

$$V_1(p,z) = \frac{\alpha_1+\alpha_2}{\alpha_2}\mathrm{e}^{p(1+\lambda_1)^{1/2}z} + \frac{\alpha_2-\alpha_1}{\alpha_2}\mathrm{e}^{-p(1+\lambda_1)^{1/2}z} + \frac{\beta_1+\beta_2}{\alpha_2}\mathrm{e}^{p(1+\lambda_2)^{1/2}z}$$
$$+ \frac{\beta_2-\beta_1}{\alpha_2}\mathrm{e}^{-p(1+\lambda_2)^{1/2}z} + \frac{\gamma_1+\gamma_2}{\alpha_2}\mathrm{e}^{p(1+\lambda_3)^{1/2}z} + \frac{\gamma_2-\gamma_1}{\alpha_2}\mathrm{e}^{-p(1+\lambda_3)^{1/2}z}. \tag{40}$$

In view of (22)–(24) the sums $\alpha_1+\alpha_2$, $\beta_1+\beta_2$ and $\gamma_1+\gamma_2$ are $O(\mathrm{e}^{-pH})$, $O(\mathrm{e}^{-Ta^{1/2}H})$, $O(\mathrm{e}^{-Ta^{1/2}H})$, respectively; but these small terms must be evaluated carefully because they are multiplied by large exponents in (40). To this end (21) is rearranged as

$$\frac{(\alpha_1+\alpha_2)}{\alpha_2}\mathrm{e}^{p(1+\lambda_1)^{1/2}H} + \frac{(\beta_1+\beta_2)}{\alpha_2}\mathrm{e}^{p(1+\lambda_2)^{1/2}H} + \frac{(\gamma_1+\gamma_2)}{\alpha_2}\mathrm{e}^{p(1+\lambda_3)^{1/2}H}$$
$$= \left(\frac{\alpha_1}{\alpha_2}-1\right)\mathrm{e}^{-p(1+\lambda_1)^{1/2}H} - 2\frac{\beta_2}{\alpha_2}\mathrm{e}^{-p(1+\lambda_2)^{1/2}H} - 2\frac{\gamma_2}{\alpha_2}\mathrm{e}^{-p(1+\lambda_3)^{1/2}H}; \tag{41a}$$

$$\frac{(\alpha_1+\alpha_2)}{\alpha_2}\lambda_1\mathrm{e}^{p(1+\lambda_1)^{1/2}H} + \frac{(\beta_1+\beta_2)}{\alpha_2}\lambda_2\mathrm{e}^{p(1+\lambda_2)^{1/2}H} + \frac{(\gamma_1+\gamma_2)}{\alpha_2}\lambda_3\mathrm{e}^{p(1+\lambda_3)^{1/2}H}$$
$$= \left(\frac{\alpha_1}{\alpha_2}-1\right)\lambda_1\mathrm{e}^{-p(1+\lambda_1)^{1/2}H} - 2\frac{\beta_2}{\alpha_2}\lambda_2\mathrm{e}^{-p(1+\lambda_2)^{1/2}H} - 2\frac{\gamma_2}{\alpha_2}\lambda_3\mathrm{e}^{-p(1+\lambda_3)^{1/2}H}; \tag{41b}$$

$$\frac{(\alpha_1+\alpha_2)}{\alpha_2}\frac{\lambda_1}{(1+\lambda_1)^{1/2}}\mathrm{e}^{p(1+\lambda_1)^{1/2}H} + \frac{(\beta_1+\beta_2)}{\alpha_2}\frac{\lambda_2}{(1+\lambda_2)^{1/2}}\mathrm{e}^{p(1+\lambda_2)^{1/2}H}$$
$$+ \frac{(\gamma_1+\gamma_2)}{\alpha_2}\frac{\lambda_3}{(1+\lambda_3)^{1/2}}\mathrm{e}^{p(1+\lambda_3)^{1/2}H} = -\left(\frac{\alpha_1}{\alpha_2}-1\right)\frac{\lambda_1}{(1+\lambda_1)^{1/2}}\mathrm{e}^{-p(1+\lambda_1)^{1/2}H}$$
$$+ 2\frac{\beta_2}{\alpha_2}\frac{\lambda_2}{(1+\lambda_2)^{1/2}}\mathrm{e}^{-p(1+\lambda_2)^{1/2}H} + 2\frac{\gamma_2}{\alpha_2}\frac{\lambda_3}{(1+\lambda_3)^{1/2}}\mathrm{e}^{-p(1+\lambda_3)^{1/2}H}. \tag{41c}$$

Since α_1/α_2 is a known function (see (22)) we actually have a system for three variables: $\alpha_1+\alpha_2$, $\beta_1+\beta_2$ and $\gamma_1+\gamma_2$. The solution, in view of (20), is

$$\frac{(\alpha_1+\alpha_2)}{\alpha_2}=\left[\frac{c_{11}}{c_{00}}\left(\frac{\alpha_1}{\alpha_2}-1\right)\frac{e^{-p(1+\lambda_1)^{1/2}H}}{e^{p(1+\lambda_1)^{1/2}H}}+\frac{c_{21}}{c_{00}}\frac{\lambda_1-\lambda_3}{\lambda_3-\lambda_2}\frac{e^{-p(1+\lambda_2)^{1/2}H}}{e^{p(1+\lambda_1)^{1/2}H}}+\frac{c_{31}}{c_{00}}\frac{\lambda_2-\lambda_1}{\lambda_3-\lambda_2}\frac{e^{-p(1+\lambda_3)^{1/2}H}}{e^{p(1+\lambda_1)^{1/2}H}}\right]; \tag{42a}$$

$$\frac{(\beta_1+\beta_2)}{\alpha_2}=\left[\frac{c_{12}}{c_{00}}\left(\frac{\alpha_1}{\alpha_2}-1\right)\frac{e^{-p(1+\lambda_1)^{1/2}H}}{e^{p(1+\lambda_2)^{1/2}H}}+\frac{c_{22}}{c_{00}}\frac{\lambda_1-\lambda_3}{\lambda_3-\lambda_2}\frac{e^{-p(1+\lambda_2)^{1/2}H}}{e^{p(1+\lambda_2)^{1/2}H}}+\frac{c_{32}}{c_{00}}\frac{\lambda_2-\lambda_1}{\lambda_3-\lambda_2}\frac{e^{-p(1+\lambda_3)^{1/2}H}}{e^{p(1+\lambda_2)^{1/2}H}}\right]; \tag{42b}$$

$$\frac{(\gamma_1+\gamma_2)}{\alpha_2}=\left[\frac{c_{13}}{c_{00}}\left(\frac{\alpha_1}{\alpha_2}-1\right)\frac{e^{-p(1+\lambda_1)^{1/2}H}}{e^{p(1+\lambda_3)^{1/2}H}}+\frac{c_{23}}{c_{00}}\frac{\lambda_1-\lambda_3}{\lambda_3-\lambda_2}\frac{e^{-p(1+\lambda_2)^{1/2}H}}{e^{p(1+\lambda_3)^{1/2}H}}+\frac{c_{33}}{c_{00}}\frac{\lambda_2-\lambda_1}{\lambda_3-\lambda_2}\frac{e^{-p(1+\lambda_3)^{1/2}H}}{e^{p(1+\lambda_3)^{1/2}H}}\right], \tag{42c}$$

where $((\alpha_1/\alpha_2)-1)$ is determined from (22),

$$c_{00}=\lambda_3\frac{\lambda_2-\lambda_1}{(1+\lambda_3)^{1/2}}+\lambda_2\frac{\lambda_1-\lambda_3}{(1+\lambda_2)^{1/2}}+\lambda_1\frac{\lambda_3-\lambda_2}{(1+\lambda_1)^{1/2}}, \tag{43}$$

and c_{ij}, $i,j=1,2,3$, stand for algebraic expressions, which are separated from the exponents in the determinants. Thus

$$c_{11}=\lambda_3\frac{\lambda_2-\lambda_1}{(1+\lambda_3)^{1/2}}+\lambda_2\frac{\lambda_1-\lambda_3}{(1+\lambda_2)^{1/2}}+\lambda_1\frac{\lambda_2-\lambda_3}{(1+\lambda_1)^{1/2}}, \tag{44a}$$

$$c_{12}=2\lambda_1\frac{\lambda_3-\lambda_1}{(1+\lambda_1)^{1/2}},\quad c_{13}=2\lambda_1\frac{\lambda_1-\lambda_2}{(1+\lambda_1)^{1/2}}. \tag{44b, c}$$

It can be concluded from (42) and (A 23) that the contributions of the second and third terms on the right-hand sides of (42) are, as compared with the first term, exponentially small, $O(e^{-HTa^{1/2}})$, for $p\leqslant 1.12\,Ta^{1/2}$. For $p\geqslant 1.12\,Ta^{1/2}$, due to (A 22)–(A 23), these two terms in (42) after substitution in (40) contribute actually $O(e^{-HTa^{1/2}})$. Consequently, these terms are neglected. After this simplification, and on account of (42)–(43) and (20), (40) yields, again with $O(e^{-HTa^{1/2}})$ accuracy,

$$\begin{aligned}V_1(p,z)=&\frac{c_{11}}{c_{00}}\left(\frac{\alpha_1}{\alpha_2}-1\right)e^{p(1+\lambda_1)^{1/2}(z-2H)}+\left(\frac{\alpha_1}{\alpha_2}-1\right)e^{-p(1+\lambda_1)^{1/2}z}\\&+\frac{c_{12}}{c_{00}}\left(\frac{\alpha_1}{\alpha_2}-1\right)e^{-p(1+\lambda_1)^{1/2}H+p(1+\lambda_2)^{1/2}(z-H)}+2\frac{\lambda_1-\lambda_3}{\lambda_3-\lambda_2}e^{-p(1+\lambda_2)^{1/2}z}\\&+\frac{c_{13}}{c_{00}}\left(\frac{\alpha_1}{\alpha_2}-1\right)e^{-p(1+\lambda_1)^{1/2}H+p(1+\lambda_3)^{1/2}(z-H)}+2\frac{\lambda_2-\lambda_1}{\lambda_3-\lambda_2}e^{-p(1+\lambda_3)^{1/2}z}.\end{aligned} \tag{45}$$

In a similar manner the integral representation kernels for the other flowfield variables have been reformulated to preserve the $O(e^{-HTa^{1/2}})$ accuracy.

2.5. *Choice of k and other validity considerations*

An essential task in the solution is choosing of k in the expansion (30). To fix it for the unbounded configuration (see VU) a principle was put forward, namely, that the

pressure distribution on the disk, $P(r, z = 0)$, has the same singularity at $r \to 1$ as in the non-rotational case in which (see Ray 1936):

$$P(r, z = 0) = \frac{4}{\pi}\int_0^\infty J_0(rp)\sin p\,\mathrm{d}p = \frac{4}{\pi}\frac{1}{(1-r^2)^{1/2}} \quad \text{for} \quad r < 1. \tag{46}$$

The singularity originates from the geometric configuration, i.e. the edge of the disk. In the infinitesimally small vicinity of the edge the flow-field structure (not the amplitude) must be determined by the edge, the effect of rotation (represented by Ta) being not of primary importance because the Coriolis terms are there much smaller than the viscous shear and the pressure gradient. It is this consideration that leads to the conclusion that, from the physical point of view, the correct value of k in the unbounded case is $\frac{1}{2}$, independent of Ta.

The pressure distribution in the disk plane $z = 0$, for the present case, in view of (15), (20) and (36) results in the same formula as in the unbounded case:

$$P(r, z = 0) = \int_0^\infty J_0(rp) f(p)\,\mathrm{d}p, \tag{47}$$

but now f depends on H. Extending the previous consideration we claim that the type of singularity cannot be influenced by the bounding walls, but rather is determined by the local near-edge balance. In view of this argument, and since it was proved in VU that the required type of singularity in (47) is provided by $k = \frac{1}{2}$, in (30) we have to take the same k.

The evident considerations in choosing k are the provision of: convergence of the integrals in (33); existence of the solution for the infinite linear system (31)–(32); convergence of (30) for any p.

Consider now the kernel function $\tilde{G}$, and denote by the subscript ∞ the unbounded case values. It has been shown in VU that $\tilde{G}_\infty$ can be represented as $\tilde{G}_\infty(p) = G_\infty(s)/p$, where $s = 4Ta^2/p^4$, and that

$$0 < 1 - G_\infty(s) = O(s). \tag{48}$$

From (34)–(37) and (22), it can be concluded that $\tilde{G}(p) = G(s; H)/p$ and that for any finite H

$$0 < G(s; H) < G_\infty(s) < 1, \tag{49}$$

and in particular, in view of (38) which is correct asymptotically along with (24) for $p \gg Ta^{1/2}$,

$$G_\infty(s) - G(s; H) < O(\mathrm{e}^{-pH}) \quad \text{for} \quad s \to 0. \tag{50}$$

Combining two last results one has

$$1 - G(s; H) = O(s) \quad \text{for} \quad s \to 0. \tag{51}$$

On account of the last formula it can be concluded from (33) that the best rate of convergence for $L_{n,m}$ is attained by $k = \frac{1}{2}$. Whereas, following Kantorovich & Krylov (1964, chapter 1) we verified that the 'generalized result' of Koch is applicable to (31)–(32) with $k = \frac{1}{2}$, for any Ta. Consequently, the solution a_m is unique and can be obtained as a limit of the solutions for truncated systems of N equations with N variables as $N \to \infty$. Fast convergence of a_m was observed numerically.

Another concern is the global validity of the process of solving the dual-integral equation in view of the errors introduced at an earlier stage by the approximate

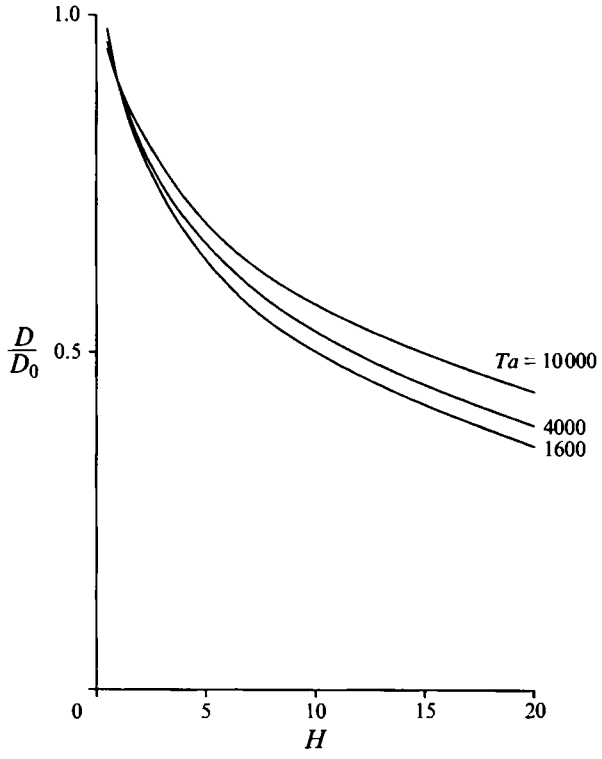

FIGURE 2. Reduced drag *vs.* H in a short container, present theory. ($D_0 = \frac{1}{2}\pi Ta^{3/2}$.)

asymptotic solution of the system (21). We estimated that the effect of these errors on the kernel $\tilde{G}$ is on the margin of the resolution of the double-precision calculations in the range of Ta and H used here. The same order of magnitude of these errors is kept for the coefficients (33) of the linear system (31)–(32). The computations performed showed that the truncated linear systems (31)–(32) are well-conditioned, thus the error in the resulting a_m is also small, and therefore the accuracy of the expansion (30) of the solution function $f(p)$ is practically unaffected by the approximate asymptotic solution of the system (21). Finally, we notice that the accuracy of α_2, see (34), and of the integrands in (11)–(13) (after reformulations like that of (40)) is also kept at $O(e^{-H\,Ta^{1/2}})$.

Upon reviewing all these stages of the solution process, we conclude that the procedure used in this work is valid and reliable for the treated range of parameters. The dominant inaccuracies in the final results are contributed by the unavoidable truncation of the expansion (30) and by the numerical evaluation of the integrals.

The calculation of the drag for $k = \frac{1}{2}$ results in the same formula as for unbounded case (denoting by T and by B the upper and lower flow regions):

$$D = 2\pi \int [P^T(z=0) - P^B(z=0)]\, r\, dr = 4(2\pi)^{1/2} a_0. \tag{52}$$

Some results are presented below.

3. Results for small and moderate H

For large Ta and non-large H, as specified later, the flow field above (and below) the body can be envisaged as a quite simple almost inviscid 'core', in which P, u, v are z-independent, embedded in horizontal Ekman layers and vertical Stewartson layers (Moore & Saffman 1968, 1969). A sharper consideration, see below, reveals the following two points. First, this simple structure appears when the inner Stewartson layer is very thin, i.e. $(H/Ta)^{1/3} \ll 1$ (say, $H < Ta/1000$). Secondly, in this asymptotic range we actually can still distinguish between three different cases: the geostrophic, quasi-geostrophic and Ekman-free quasi-geostrophic approximations, which correspond to very small, moderately small and $O(1)$ thickness of the outer Stewartson layer ($\approx \epsilon$, see below). In the geostrophic approximation the radial volume transport in the core, uH, is assumed $o(1)$ and afterwards neglected, but in the quasi-geostrophic flow the contribution of uH is accounted for as an $O(1)$ term. The contribution of the Ekman layers to the radial volume transport changes from dominant to unimportant from the first to the last case. Sharper distinctions between these ranges are given below.

In the simplest 'short container' model the core is dominated by the geostrophic (inviscid) balance, i.e. the radial Coriolis component $-2v$ is counteracted by the pressure gradient $-\mathrm{d}P/\mathrm{d}r$ and the azimuthal Coriolis term $2u$ vanishes. Consequently, there is no radial mass flow in the core, and the geostrophic swirl velocity in the core is readily obtained by the requirement that the Ekman layers perform the entire radial mass transport produced by the axial advance of the body; for a disk this yields (see, for instance, Ungarish 1993, §3.8, and Appendix B below)

$$\omega_0 = -\tfrac{1}{2}Ta^{1/2}. \tag{53}$$

Subsequent use of the geostrophic balance $-2\omega_0 r = -\mathrm{d}P/\mathrm{d}r$ and of (52) gives the drag of the geostrophic core for a disk as

$$D_0 = \tfrac{1}{2}\pi Ta^{3/2}. \tag{54}$$

Hereafter, the subscript 0 denotes the geostrophic result; in particular, D_0 is the drag obtained under the assumption that $H/Ta^{1/2} \to 0$ so that the geostrophic domain covers the entire disk. By this method Moore & Saffman (1968) obtained the geostrophic drag on a rising sphere as $D_0 = (43\pi/105)\,Ta^{3/2}$. (On the spherical particle the Ekman layers become 'inclined' as r approaches 1, hence thicker and more efficient for mass transport; therefore ω_0 decreases with r and the drag is smaller than on a disk.)

Let us compare the presently obtained 'exact' result for the drag, D, see (52), with the predictions of Moore & Saffman's type of approximation, D_0, for different values of H and Ta. In figure 2 values of D/D_0 *vs.* H are displayed for $Ta = 1600, 4000, 10000$ and $0.5 \leqslant H \leqslant 20$. As can be easily seen the exact result for drag is close to D_0 only if H does not increase beyond the value of 1–2. For larger H the ratio D/D_0 decreases fast with increase of H. Thus as H reaches 5, although $H/Ta^{1/2}$ is as small as 0.05 for $Ta = 10000$, the ratio D/D_0 drops to 0.7; as H reaches 20 and $H/Ta^{1/2} = 0.2$ for the same value of $Ta = 10000$, $D/D_0 < 0.5$. So one can judge how narrow in practice is the range of applicability of the asymptotic result D_0 even for Ta as big as 10000.

We emphasize that both D and D_0 are outcomes of the linear theory (i.e. the $Ro = 0$ limit). We attempt to explain the discrepancy between them. The fact that D is smaller than D_0 can be readily justified. We recall that in the outer Stewartson layer, of typical thickness

$$\epsilon = (\tfrac{1}{2}H/Ta^{1/2})^{1/2}, \tag{55}$$

see Moore & Saffman (1969) and Appendix B, the swirl velocity decays exponentially from ω_0 to zero. Consequently, the ring of thickness ϵ near the disk's edge contributes to the drag significantly less than assumed for D_0, i.e. we can expect that $D/D_0 = 1-O(\epsilon)$. This is, qualitatively, in agreement with figure 2.

The quasi-geostrophic core (plus Ekman layers) model is employed for a quantitative verification of this trend. This is obtained by the incorporation of the leading shear term in the radial momentum balance of the core, see Appendix B, so that the core is able to participate in the radial mass transfer in addition to the Ekman layers; for small ϵ this is equivalent to the addition of the outer Stewartson ($\frac{1}{4}$) layer to the geostrophic core. (This extension of the geostrophic core model is not difficult because the z-independence of u, v and P outside the Ekman layers remains valid, and the subsidiary boundary condition $v(r=1,z)=0$ to the leading order is evident in the z-symmetric geometry.) This improved, quasi-geostrophic core approximation, yields, for $0^+ < z < H^-$,

$$\omega = -\tfrac{1}{2}Ta^{1/2}\left[1-\frac{I_1(r/\epsilon)}{rI_1(1/\epsilon)}\right], \quad u = \frac{1}{2H}\frac{I_1(r/\epsilon)}{I_1(1/\epsilon)}, \tag{56}$$

and

$$D = \frac{\pi}{2}Ta^{3/2}\left[1-4\epsilon\frac{I_2(1/\epsilon)}{I_1(1/\epsilon)}\right]. \tag{57}$$

To understand the trends introduced by the parameter H, via the combination ϵ, we approximate the foregoing results for small and large values of ϵ.

For $\epsilon \ll 1$ we obtain

$$\omega \approx \omega_0\left[1-\exp\left(\frac{r-1}{\epsilon}\right)\right]; \quad u \approx \frac{1}{2H}\exp\left(\frac{r-1}{\epsilon}\right) \quad \text{for} \quad \epsilon \ll r \leqslant 1; \tag{58}$$

$$\omega(r=0) \approx \omega_0\left[1-\left(\frac{\pi}{2}\right)^{1/2}\epsilon^{-3/2}\,\mathrm{e}^{-1/\epsilon}\right]; \tag{59}$$

$$D \approx D_0(1-4\epsilon). \tag{60}$$

And for $\epsilon > 1$ we obtain

$$\omega \approx \omega_0\frac{1}{8\epsilon^2}(1-r^2) = -\frac{1}{8}\frac{Ta}{H}(1-r^2); \quad u \approx \frac{r}{2H}; \tag{61}$$

$$D \approx \frac{\pi}{24}Ta\frac{Ta}{H}. \tag{62}$$

Here, again, the subscript 0 indicates the geostrophic model in which the shear outside the Ekman layers was omitted, i.e. the assumption $\epsilon \to 0$, see (53)–(54).

It is worth mentioning that the approximations (61)–(62) actually represent a special physical situation: the Ekman layers do not contribute to the motion and the entire radial mass transport is performed in the core by the $2\pi urH$ term. This is the Ekman-free quasi-geostrophic case. For $\epsilon > 1$ the difference between this and the full quasi-geostrophic model is less than $(6/\epsilon^2)\%$ in drag and less than $(12/\epsilon^2)\%$ in swirl velocity. Moreover, we note that (62) and (61) coincide with the leading term in Hocking *et al.* (1979, equations (5.3) and (5.4)), corresponding results obtained for the lower limit of the 'long container' analysis. This overlap of these two different approaches strengthens the reliability of the 'short container' theory, in the enhanced quasi-

geostrophic form; furthermore, the 'long container' theory is apparently valid for $H/Ta^{1/2} > 1$ (not just $H/Ta^{1/2} \gg 1$).

In view of the insight supplied by (60) and (62) the behaviour observed in figure 2 is no longer surprising. However, although (57) gives the correct trend, it turns out, from comparisons with exact solutions, see table 1 in Appendix B, that its accuracy in typical practical cases is low. This is because the H, Ta range of applicability of the quasi-geostrophic drag is determined by two requirements: (*a*) the omitted inner Stewartson layer is very thin, $(H/Ta)^{1/3} \ll 1$ (say, $H < 10^{-3}Ta$), and (*b*) the outer Stewartson layer (or domain) is much thicker, $(H/Ta)^{1/3}/\epsilon \ll 1$ (say, $H > 10^{6}Ta^{-1/2}$). The concurrent fulfillment of (*a*) and (*b*) is theoretically possible (for, say, $Ta > 10^{6}$) but is unattainable in known experimental configurations, and even out of the range of the present computations. In practice one or both conditions are compromised (not completely violated) but the drag is very sensitive to errors near the rim and the accuracy of the improvement over the geostrophic model is lost when conditions (*a*) and (*b*) are not strictly satisfied. The conclusion is that 'exact' solutions are necessary for obtaining the linear drag in a 'short container' configuration with a tolerable error; this is practically relevant because really large values of Ta seem unattainable in industrial and experimental devices.

Indeed, consider the experiments of Maxworthy (1968); he used spherical particles of two diameters and covered different values of Ta and Ro, for $H \approx 5$ and 10. His results are displayed in figure 3 as drag *vs.* $Ro\,Ta^{2/3}$. We see that the measured values are about 20% less than Moore & Saffman's D_0 when $Ro\,Ta^{2/3} < 1$. This discrepancy with theory has been attributed to the influence of unavoidable nonlinear effects, i.e. not sufficiently small Ro. An order-of-magnitude estimate of the contribution of the convection terms in the geostrophic core region yields the condition $Ro \ll Ta^{-1/2}$. However, the estimate of Moore & Saffman (1968), based on the flow in the Stewartson shear layers is much more restrictive: $Ro \ll Ta^{-5/7}\,H^{3/7}$ ($\approx Ta^{-5/7}$). The fact that the experimental points of Maxworthy do not satisfy the latter restriction led to the above-mentioned explanation of the drag discrepancy.

Although this consideration is formally correct, we claim that it is over-restrictive. The relative contribution of the narrow shear layers to the drag is much smaller than that of the core. Hence we suggest that a more practical criterion for the applicability of the linear theory is one demanding that the convection in the core is small, $Ro \ll Ta^{-1/2}$, while that in the shear layers does not exceed $O(1)$. The combination can be expressed as $Ro < Ta^{-5/7}$.

This argument brings us to the idea that, for the experimental points with $Ro \leqslant Ta^{-2/3} \ll Ta^{-1/2}$ at least, the departure of the measured drag from D_0 is not caused by the convective terms. Instead, we suggest that the influence of H on the system could cause the discrepancy (in the experiments $0.1 < \epsilon < 0.3$) and attempt to verify this explanation via a comparison based on the present linear outcomes with Maxworthy's experiments. This is not a straightforward task since (*a*) the particle geometry is different, and (*b*) the reported experimental points are not labelled with the appropriate values of H. To proceed, we assume that D/D_0 for disk and sphere are close. For $Ta = 26000$ (the maximal available value) the experimental results are in the range $D/D_0 = 0.87-0.90$; on the other hand, the present theory for $H = 5$ predicts $D/D_0 = 0.89$. It is likely that these experiments represent exactly this value of H (the reported experimental error is $\pm 2.5\%$). For $Ta = 25000$ two results, 0.90 and 0.74, are displayed in the experimental points. The appropriate present calculations for $H = 5$ and 10 result in $D/D_0 = 0.89$ and 0.73.

Maxworthy also reports significant discrepancies of the swirl velocity in the core

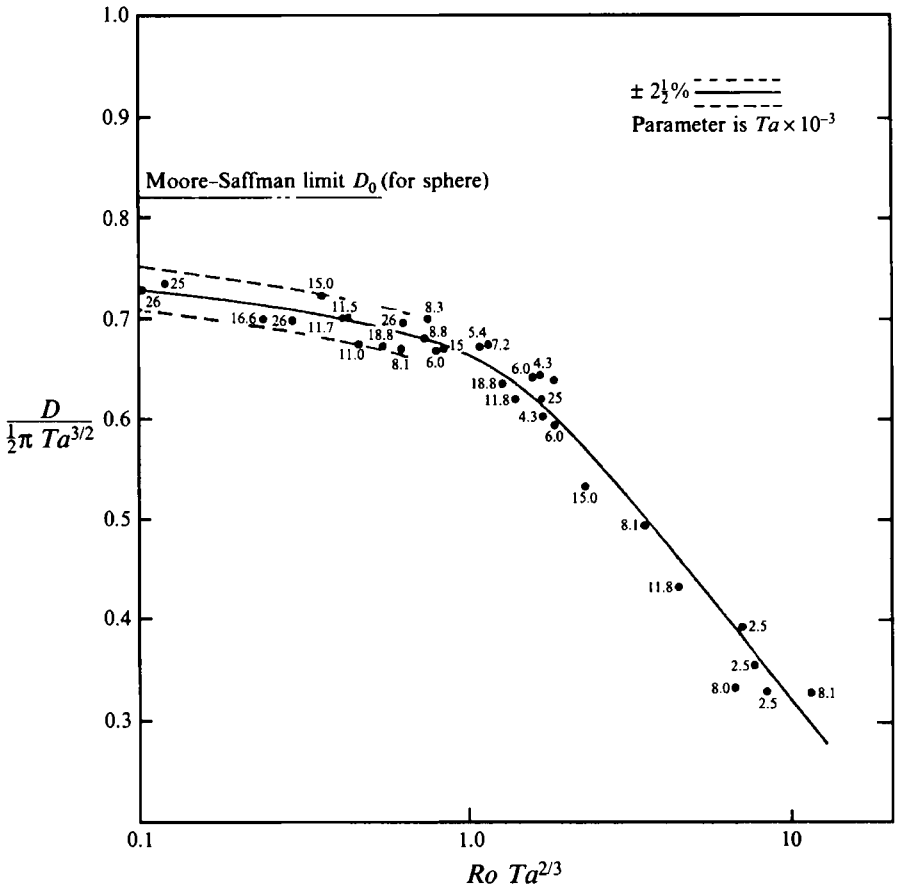

FIGURE 3. Drag *vs.* 'effective Rossby number', experiments of Maxworthy (1968).

with the asymptotic value ω_0. However, using (56) we readily calculate that the ratio $\omega(r=0)/\omega_0$ decreases from 0.997 to 0.73 when ϵ changes from 0.1 to 0.3. This is consistent with the experimental results (figure 10 of Maxworthy 1968) but the scatter is too large for a quantitative comparison.

In view of all this it seems appropriate to attribute the real departure of the drag in these experiments from D_0, for smallest Ro and largest Ta, mainly to the influence of H (actually, to the non-vanishing ϵ), a possibility which was overlooked. In other words, Maxworthy's (1968) experiments seem to rather confirm the linear theory; the nonlinear effects seem to become influential on the drag when $Ro\, Ta^{2/3} > 1$.†

Consider now some features of the flow field, in particular the behaviour of the angular velocity, ω, and of the stream function in the meridional plane, ψ, with increase of H. It is convenient to introduce the parameter

$$\delta = H/Ta. \tag{63}$$

The exact results show that for large values of Ta, if δ is less than about 0.05, the

† Investigations performed after the completion of this paper lend further support to this conjecture, as well as to the assumption that D/D_0 for disk and sphere are close in the present range of parameters, Ungarish (1995).

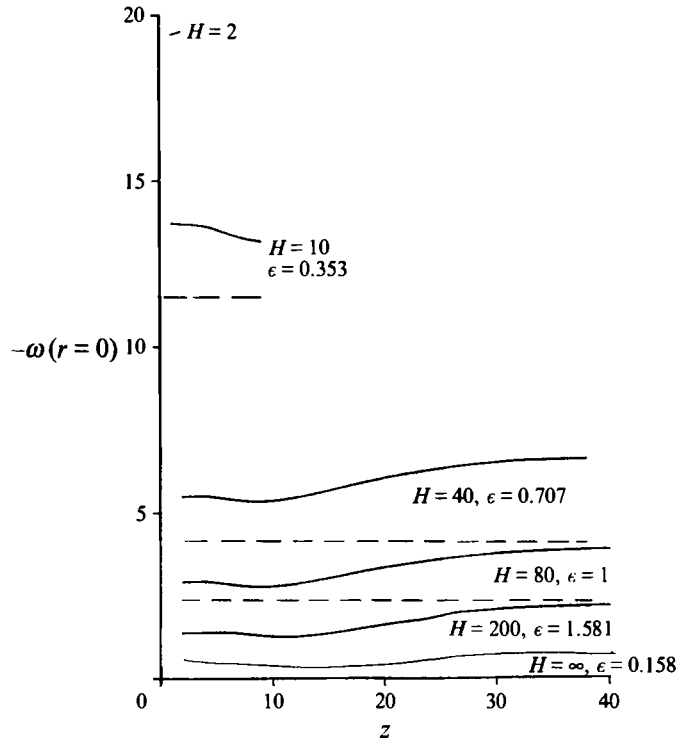

FIGURE 4. Angular velocities at various values of z at $r = 0$ for different values of H at $Ta = 1600$. Exact (——) and quasi-geostrophic (– – –) results. ($\omega_0 = -20$.)

variable ω in the core is quite z-independent. This is illustrated in figure 4, where it is also seen that the 'exact' value of $\omega(r = 0, z)$ is in good agreement with the quasi-geostrophic approximation (56). This is a mutual confirmation of the present outcomes and of the asymptotic ones. We emphasize that the agreement in $\omega(r = 0)$ is better than for drag. This can be justified, for small ϵ, as follows: the quasi-geostrophic model misses the details of the $\frac{1}{3}$ layer, but the contribution of the $\frac{1}{3}$ layer when $(H/Ta)^{1/3}/\epsilon$ is not small is expected to be significant near the rim $r = 1 - O(\epsilon)$, from where the major drag modifications come, not near the axis $r = 0$.

A striking feature of the flow field is the recirculating motion in the inner Stewartson ($\frac{1}{3}$) layer, predicted by Moore & Saffman (1969). To solve the flow field in this layer Moore & Saffman simplified the momentum equations and showed that the corresponding solutions are non-unique, fail in the Ekman layer and have a sharp edge singularity. To choose the unique solution the principle of minimal singularity of velocity of Kutta–Joukowsky type was applied. Under this conjecture, it was found by Moore & Saffman that the axial velocity in the $\frac{1}{3}$ layer must be $O(Ta^{5/12}/H^{1/6})$. This velocity in the layer of width $O[(H/Ta)^{1/3}]$ induces a large, $O[(H^2Ta)^{1/12}]$, mass circulation, which must be a confined recirculating motion because the mass flux induced by the motion of the particle in all the regions of the flow field is no larger than $O(1)$. In other words, the leading order-of-magnitude motion in the $\frac{1}{3}$ layer is expected to be an internal recirculation.

In our 'exact' solution a recirculation was indeed observed, with the following features. When H is of order unity, the smallest value of Ta for which recirculation arises is $Ta \approx 1000$. For a constant value of H the recirculation increases with Ta (see

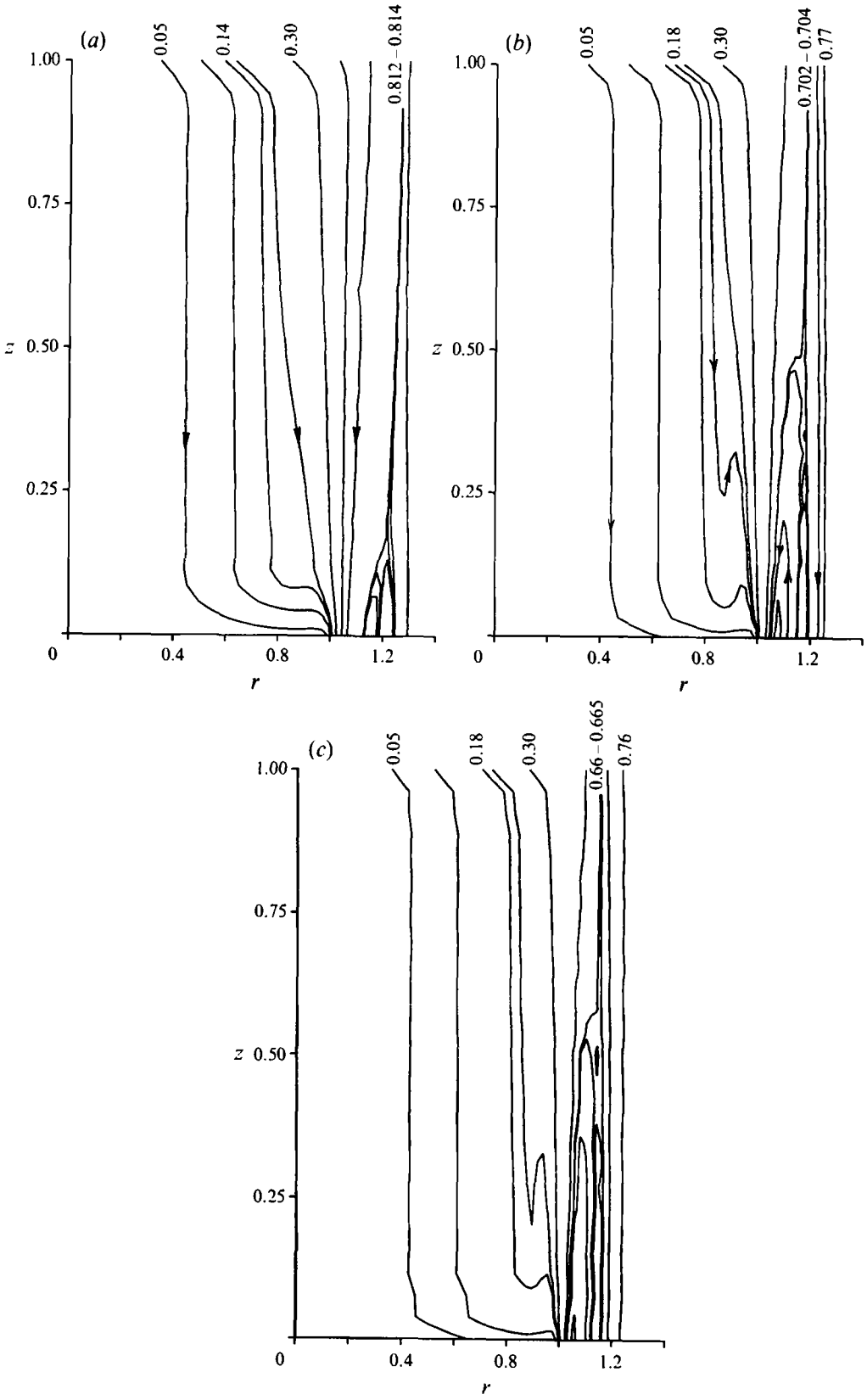
(a)
0.05
0.14
0.30
0.812 – 0.814
1.00
0.75
z 0.50
0.25
0
0.4
0.8
1.2
r
(b)
0.05
0.18
0.30
0.702 – 0.704
0.77
1.00
0.75
z 0.50
0.25
0
0.4
0.8
1.2
r
(c)
0.05
0.18
0.30
0.66 – 0.665
0.76
1.00
0.75
z 0.50
0.25
0
0.4
0.8
1.2
r

figure 5), as predicted. However, since the maximal attainable computational values are $Ta = O(10000)$ this recirculating motion was not really dominant and its exact dependency on the quite insensitive $Ta^{1/12}$ could not be verified. For the parameters investigated here, for fixed value of Ta the recirculation decreases as H increases (contrary to the foregoing rough orders-of-magnitude estimations). Thus one can see in figure 6 that for $Ta = 6400$ while $H = 1$, 2 and 4 the recirculating flux is approximately $\psi_{rec} = 0.07$, though the entire flux in the core, conditionally defined by the stream-function value of the bifurcating line increases from 0.7 to 0.8 approximately. Additional increase of H to 6 brings to a slight decrease of the recirculating flux to $\psi_{rec} = 0.06$. Further increase of H to 8 and beyond causes a drastic reduction to complete cancellation of the recirculation.

The streamlines in figures 5(*b*, *c*) and 6 have some 'spikes' in the lower half of the container around $r \approx 0.9$, for the following reason. In the geostrophic domain, $r < 1 - O(\epsilon)$, the axial volume flux is into the Ekman layer on the disk and the axial velocity, w, is negative and $O(1)$. Below the 1/4 layer, $1 - O(\epsilon) < r < 1 - O((H\,Ta)^{-1/3})$, the disk Ekman layer expels fluid into the core, from where it is 'sucked' radially into the $\frac{1}{3}$ layer, see (58), hence w in the lower half of the container becomes positive and $O(Ta^{1/4})$. However, in the $\frac{1}{3}$ layer the net fluid transport is downward and w changes sign again. (This is not observed in figure 5(*a*) because $Ta = 1600$ is not sufficiently large for a sharp distinction between the shear layers.)

4. Results for large H

Figure 7 illustrates the changes of the stream-function contours as H increases from $O(1)$ to $O(Ta)$ for a fixed, large Ta. Here the value $Ta = 1600$ is chosen to facilitate comparison with previous unbounded case results (see VU).

As H increases the vertical shear layers, as expected, thicken; as δ reaches the value of about 0.05 a strong deflection of the near-axis streamlines in the positive radial direction upon approaching the disk occurs, and axial variations of the angular velocity appear.

Further increase of δ to about 0.08 causes a special change of the flow pattern: the central zero streamline bifurcates and a zone of recirculation ('bubble') over the disk appears. This zone first elongates with δ, but as this parameter approaches the value 0.25 (approximately) the bubble reaches an asymptote: its size and the velocities inside attain the values obtained for the unbounded configuration, which depend on Ta only. It is worth recalling that the length of the 'free' Taylor column in the unbounded configuration is $0.051\,Ta$, hence the appearance of a similar feature at $\delta \geqslant 0.08$ is not surprising; however, regarding ψ the container can be considered 'unbounded' if its lids are at least five fully developed 'free' Taylor columns away from the particle (the drag in this particular configuration is nevertheless about 30% higher than the unbounded result).

It is not without interest to notice some analogy between the influence of Ta in the unbounded case, where the onset of the bubble takes place when Ta reaches the critical value 37 and with further increase of Ta the bubble elongates, and the bounded case with the analogous parameter δ and its critical value 0.08.

The drag results for larger H can be better discussed by considering D/D_∞ for various Ta *vs.* δ. Here D_∞ denotes the 'exact' result for the unbounded configuration, as calculated in VU (which coincides with the present calculations in the limit $H \to \infty$). The typical behaviour can be inferred from figure 8: essentially, D/D_∞ increases with

FIGURE 5. The contour lines of $-\psi$ for $H = 1$ for Ta values (*a*) 1600, (*b*) 6400, (*c*) 12800.

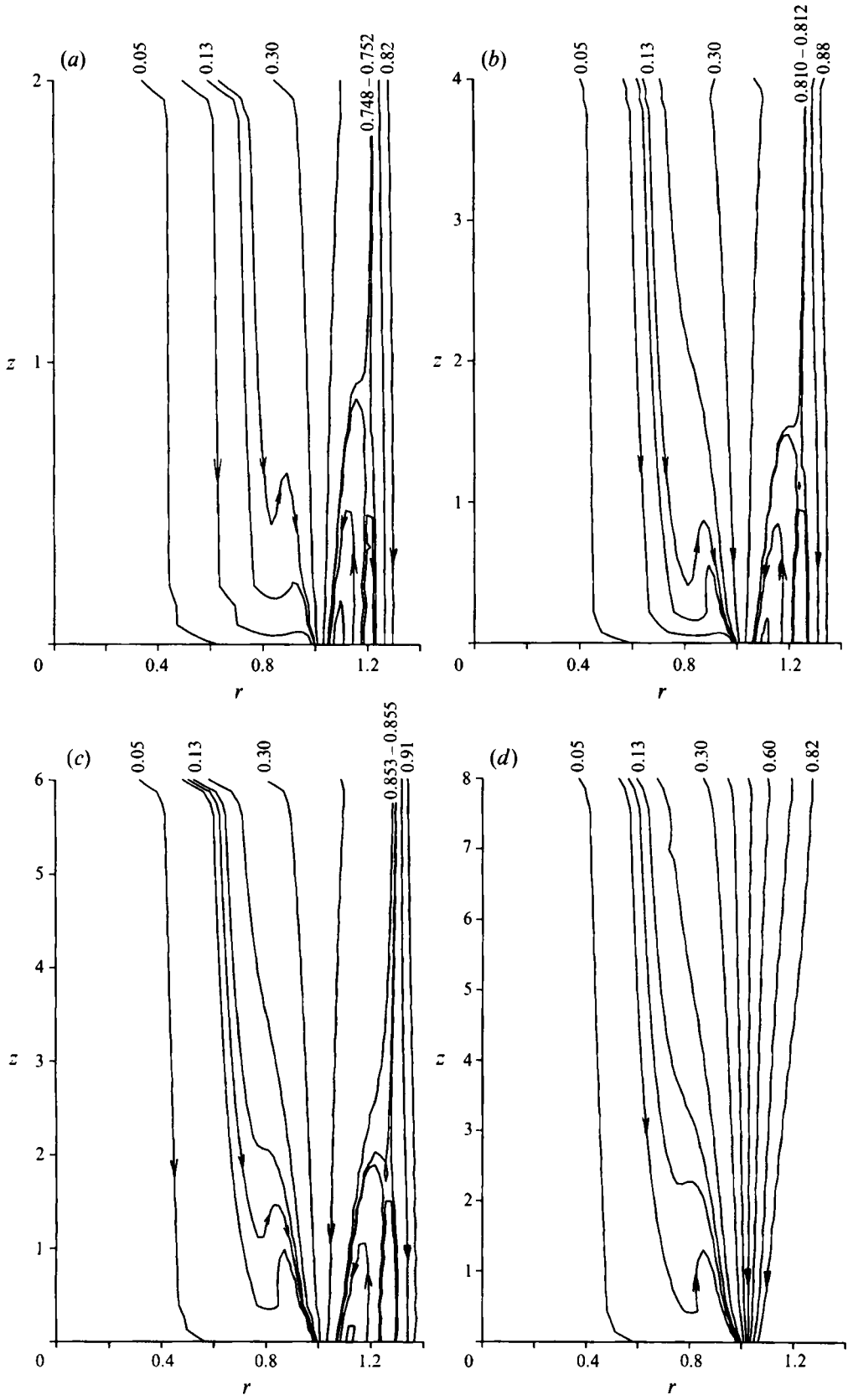
(a)
0.05
0.13
0.30
0.748 – 0.752
0.82
z
r
(b)
0.05
0.13
0.30
0.810 – 0.812
0.88
z
r
(c)
0.05
0.13
0.30
0.853 – 0.855
0.91
z
r
(d)
0.05
0.13
0.30
0.60
0.82
z
r

Ta and decreases with δ; however, for $H/Ta \geqslant 0.08$ (approximately) the curves for different Ta collapse into a single line, $F(\delta)$, i.e. D/D_∞ becomes independent of Ta.

Here the study of Hocking *et al.* (1979) is relevant. It considers the influence of the axial boundaries in a long container upon the approximation that the shear associated with the derivatives with respect to z (and thus the Ekman layers) can be neglected. This should correspond to the present results in the limit $Ta \to \infty$ with δ kept $O(1)$. The corresponding drag is here denoted D^{HMW}, and for large values of δ this drag, denoted D_∞^{HMW}, recovers the 'inviscid' unbounded case value, $(16/3)Ta$ (derived by Stewartson 1952). The drag ratio D^{HMW}/D_∞^{HMW} in this model turned out to be a function of δ only, with values given by Hocking *et al.* (in table 1 and figure 2). Comparing the drag ratio *vs.* δ of this model with that of the present 'exact' solution, see figure 8, we realize that they must also coincide for $\delta > 0.08$, i.e.

$$\frac{D}{D_\infty} = \frac{D^{HMW}}{D_\infty^{HMW}} = F(\delta) \quad \text{for} \quad \delta > 0.08. \tag{64}$$

An important conclusion is as follows. In the long container $\delta > 0.08$ the drag is influenced by two effects: the finite extent of the domain, reproduced by the finite value of δ, and the Ekman layers on the disk, reproduced by the finite value of Ta. These effects are separated:

$$D(Ta, H) = F(H/Ta) \times D_\infty(Ta). \tag{65}$$

The first factor estimates the influence of the walls without taking account of Ekman layers (Hocking *et al.*), the second is simply the 'exact' drag in an unbounded geometry, implicitly accounting for the Ekman layer on the disk (VU). Such a separation of effects at large δ could be anticipated, but the present study points out that it actually happens for $\delta > 0.08$. Moreover, it is easy to conjecture that (65) is valid for spherical and spheroidal particles, for which $D_\infty(Ta)$ is provided by Weisenborn (1985) and Tanzosh & Stone (1994). This conjecture is significant in drag comparison with experiments.

The major known discrepancy between the linear theory and experiments is in the value of the drag on a particle in a long container. Maxworthy (1970), by smoothing and extrapolating experimental data, concluded that for a very long container and large Ta the experimental drag on a spherical particle is 53% higher than the value $(16/3)\,Ta$ predicted by Stewartson (1952) (this was the only relevant linear-theory result available at that time). Hocking *et al.* attempted to attribute this discrepancy to the finite length of the container used in the experiments (actually, $0.2 < \delta < 0.8$). They used 'raw' experimental points and compared with Stewartson's inviscid drag, $(3/16)\,Ta$, augmented by $F(\delta)$; the agreement was poor, although the influence of nonlinear effects was estimated to be small.

Maxworthy and then Barnard & Pritchard (1975) suggested that significant contributions to the flow field, including the drag, can be expected from the Ekman layers. Now, through the conjectured decoupling of the effects of Ekman layer and the axial bounds, expressed in the formula (65), we can improve the comparison of Hocking *et al.* with Maxworthy's experiments. To this end we use the exact linear drag results for a sphere in an unbounded domain, $D_\infty(Ta)$, from Weisenborn or Tanzosh & Stone (instead of $(3/16)\,Ta$), and superpose the results of Hocking *et al.* Consequently, for the experimental data verified by Hocking *et al.*, beyond the above-mentioned contribution of $F(\delta)$, we found an additional increase of the theoretical drag as follows: by about 12% for the points with $Ta = 447$, $\delta \approx 0.25$ and by about 28% for the points with $Ta = 117$, $\delta \approx 0.8$ (cf. points (a) and (k) in figure 2 of Hocking

FIGURE 6. The contour lines of $-\psi$ for $Ta = 6400$ for H values (a) 2, (b) 4, (c) 6, (d) 8.

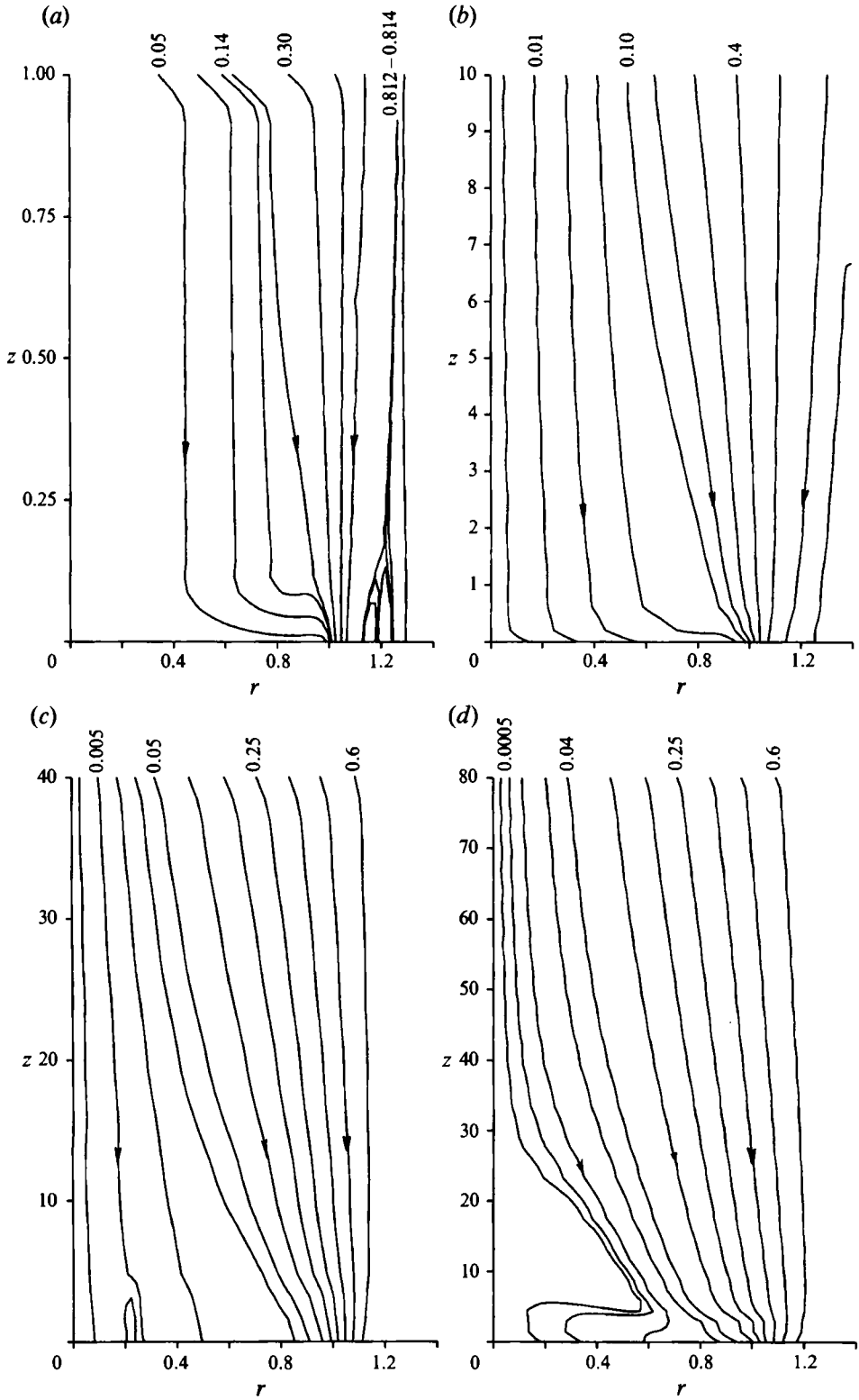

FIGURE 7 (*a–d*). For caption see facing page.

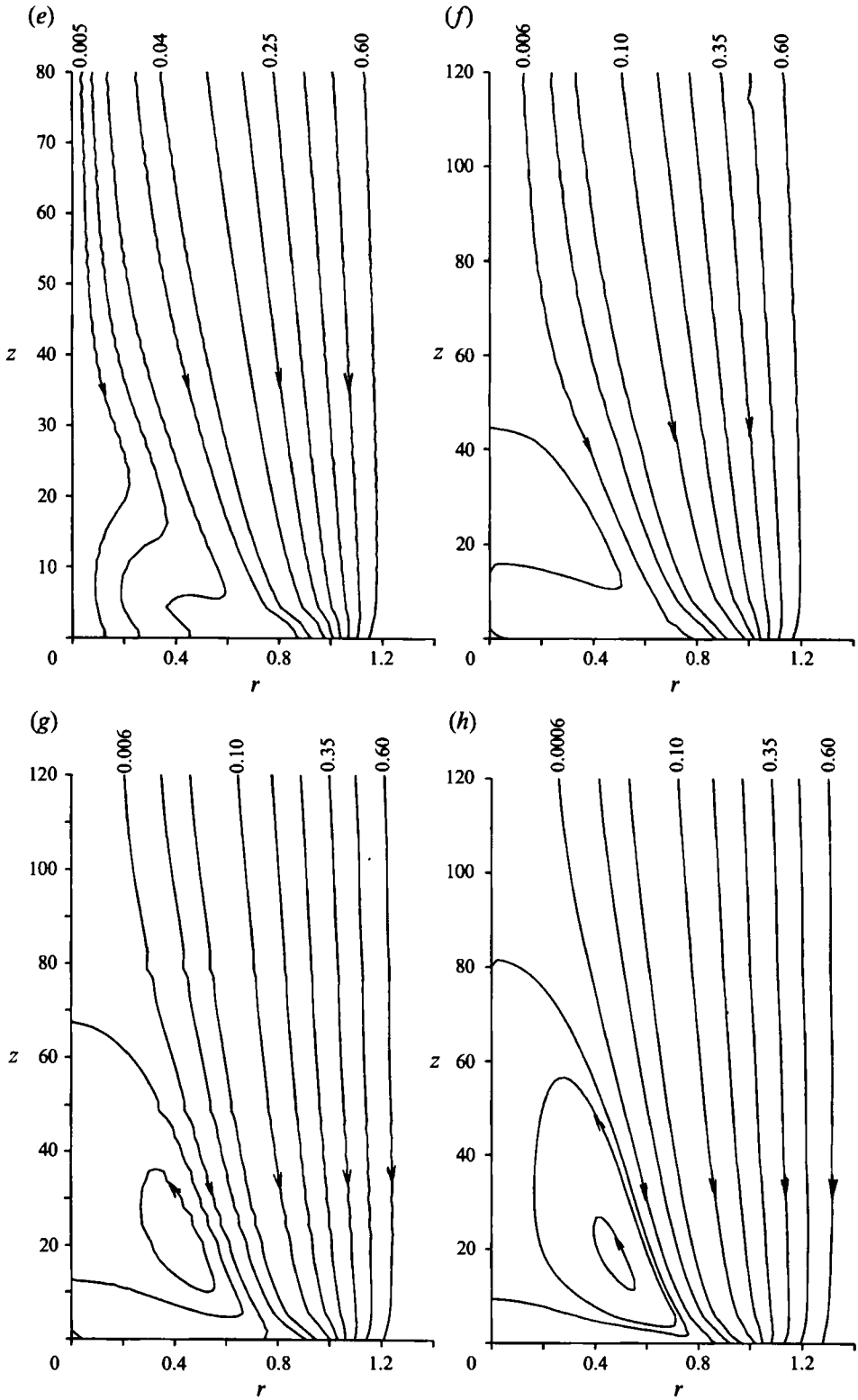

FIGURE 7. The contour lines of $-\psi$ for $Ta = 1600$ for H values (*a*) 1, (*b*) 10, (*c*) 40, (*d*) 80, (*e*) 100, (*f*) 150, (*g*) 400, (*h*) ∞.

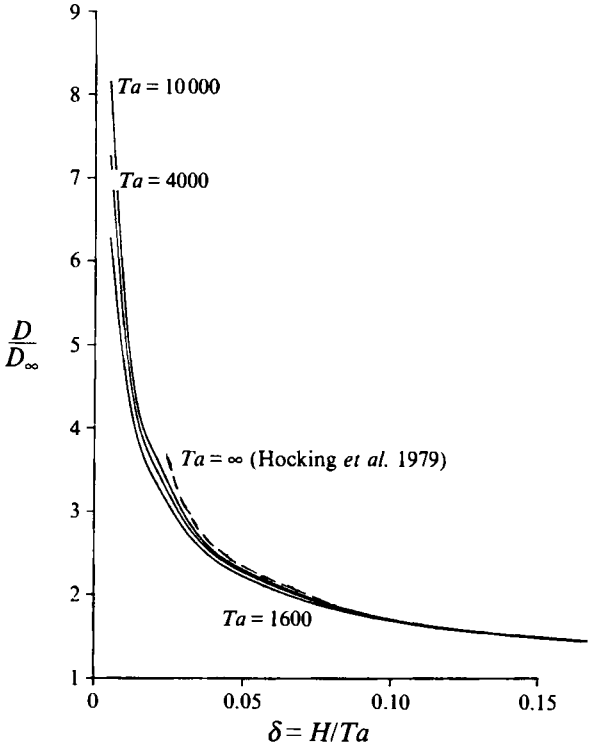

FIGURE 8. D/D_∞ *vs.* $\delta = H/Ta$, for various Ta.

et al.). However, the basic disagreement reported by Hocking *et al.* remains. It seems that the quite complete linear theory within the stable flow framework is unable to explain the essential discrepancy with these experiments.

5. Concluding remarks

The present 'exact' solution of the full linear equations facilitates the analysis of the flow field past a rising disk in rotating, axially bounded, fluid for the whole range of Taylor number, Ta, and arbitrary distance from the disk to the walls, H. A noted restriction is that the disk is supposed to be at equal distance from both walls. However, no significant departures from the present features are expected for a moderate ($\pm 30\%$ of H, say) off-middle particle position: the simplified analysis for the short cylinder in Appendix B and for the long container by Hocking *et al.* (1979) (for $H/Ta > 0.1$) indicate that the drag varies by a few percent only when the particle moves in the central third of the container; the minimum drag is in the middle position.

The method of dual-integral equations, attempted and verified in VU for the solution of the boundary value problem based on the full linear equations of motion in the unbounded configuration, has been utilized here again for the bounded container. The principle formulated in VU regarding the choice of the undetermined parameter k in Tranter's method of solution of these equations has been also successfully employed in the present case, which gives additional credence to the underlying idea.

Attention was focused on large but finite Ta, and the full range of half-container height, H, (i.e. small, moderate and large with respect to a given Ta) was covered. The

asymptotic investigations of Moore & Saffman (1968, 1969) and of Hocking *et al.* (1979) are approached by the present solution as Ta increases. The quasi-geostrophic model elaborated here improves the applicability of – and bridges the gap between – these models. However, in practical solutions (say, $Ta = O(10^3)$–$O(10^5)$) quantitative differences appear between asymptotical and exact results. The parameters $\epsilon = (\frac{1}{2}H/Ta^{1/2})^{1/2}$ and $\delta = H/Ta$ are important.

For small H (actually, small $\delta^{1/3}$) the flow-field features (in particular, the angular velocity on the axis) are described well by the asymptotic short-container model, but even for $Ta = 10000$ and $H = 1$ ($\delta^{1/3} = 0.05$, $\epsilon = 0.07$) the geostrophic drag obtained by the method of Moore & Saffman (1968) overestimates by more than 10%. In general, the asymptotic drag predictions cannot be accurate when both $\delta^{1/3}$ and ϵ are moderately small. The recirculation in the inner Stewartson layer, predicted by Moore & Saffman (1969), was qualitatively confirmed here, but the quantitative details (e.g. whether it is really of order $Ta^{1/12}$) were beyond the resolution of the present computations.

As H increases, the angular velocity in the core and the drag decrease, and the streamline structure begins to be modified. As H increases from $O(Ta^{1/2})$ to $0.08Ta$, $|\omega|$ decreases from $O(Ta^{1/2})$ to $O(1)$, and the drag from $O(Ta\,Ta^{1/2})$ to $O(Ta)$.

As δ reaches the value 0.08 the meridional flow field qualitatively changes: the recirculation 'bubble' appears, as in the unbounded configuration when $Ta > 37$. In other words, the classic 'free' Taylor column begins to form for $\delta > 0.08$. With growth of δ the bubble lengthens and widens, and when $\delta > 0.25$ (approximately) the fully developed 'free' Taylor column is recovered.

Relevant global conclusions of the present disk-particle solution could be heuristically extended to a spherical particle. The details of this extension are worthy of investigation, and it seems that the methodology used by Tanzosh & Stone (1994) for spherical and spheroidal particles in the unbounded configuration can be the appropriate means for this purpose. We note in passing that in the short container the geostrophic drag on a disk is about 22% larger than on a sphere, but in the long container the drag is slightly smaller on a disk than on a sphere.

In particular, additional light was thrown on experimental verifications of the linear-theory drag predictions performed with spherical particles. For a short container the results of Maxworthy (1968) for small Ro, although about 20% lower than the asymptotic geostrophic value of Moore & Saffman (1968) turn out to be consistent with the present analysis, in contrast with previous explanations which attributed the disagreement mainly to the influence of inertia terms.

On the other hand, for the long container, although the present study apparently incorporates all the leading effects that can be covered by the linear theory, in particular the finite Ta (Ekman layers) and the influence of the top and bottom walls, the intriguing discrepancy of about 53% in drag with Maxworthy's (1970) experimentally based conclusion remains. This fact, and the availability of the present theory that predicts the drag and velocity field as functions of the measurable H and Ta (not for asymptotic limits of these parameters as before), suggest the need – and promise efficient design and interpretation – of additional experiments.

The research was partially supported by the Fund for the Promotion of Research at the Technion, and D.V. was partially supported by the Bat Sheva de Rothschild Foundation for the Advancement of Science in Israel & Co. We thank Prof. A. Sidi for useful comments.

Appendix A. Approximations in the dual-integral equations

Here, for $p \geqslant 0$ and $HTa^{1/2} \gg 1$, some approximations used in the text, which are also essential in the asymptotic solution of (21), are developed.

First, consider the behaviour of the arguments $(1+\lambda_i)^{1/2}pH$. The λ_i are the roots of the characteristic equation

$$\lambda^3 + s\lambda + s = 0; \tag{A 1}$$

where

$$s = 4Ta^2/p^4. \tag{A 2}$$

Its three roots, by Cardano's formula, are

$$\lambda_1 = \epsilon_1 + \epsilon_2, \tag{A 3}$$

$$\lambda_2 = -\tfrac{1}{2}(\epsilon_1+\epsilon_2) + \tfrac{1}{2}\mathrm{i}\sqrt{3}(\epsilon_1-\epsilon_2), \tag{A 4}$$

$$\lambda_3 = -\tfrac{1}{2}(\epsilon_1+\epsilon_2) - \tfrac{1}{2}\mathrm{i}\sqrt{3}(\epsilon_1-\epsilon_2), \tag{A 5}$$

where

$$\epsilon_1 = \left(-\frac{s}{2} + \left(\frac{s^3}{27} + \frac{s^2}{4}\right)^{1/2}\right)^{1/3}, \tag{A 6}$$

$$\epsilon_2 = \left(-\frac{s}{2} - \left(\frac{s^3}{27} + \frac{s^2}{4}\right)^{1/2}\right)^{1/3}. \tag{A 7}$$

The asymptotics for ϵ_1 and ϵ_2 for both small and large p are readily produced. Thus for $p \to 0$, i.e. $s \to \infty$, the series expansion gives

$$\epsilon_1 = \left(-\frac{s}{2} + \left(\frac{s^3}{27}\right)^{1/2}\left(1+\frac{27}{4s}\right)^{1/2}\right)^{1/3} = \frac{s^{1/2}}{\sqrt{3}}\left(1 - \frac{3\sqrt{3}}{2s^{1/2}} + \frac{27}{8s} + \frac{1}{2s} + O\left(\frac{1}{s^2}\right)\right)^{1/3}$$

$$= \frac{s^{1/2}}{\sqrt{3}} - \frac{1}{2} + \frac{\sqrt{3}}{8s^{1/2}} + \frac{1}{2s} + O(s^{-3/2}). \tag{A 8}$$

Analogously,

$$\epsilon_2 = -s^{1/2}/\sqrt{3} - \tfrac{1}{2} - \sqrt{3}/8s^{1/2} + 1/2s + O(s^{-3/2}). \tag{A 9}$$

Hence,

$$\epsilon_1 + \epsilon_2 = -1 + 1/s + O(s^{-3/2}) \tag{A 10}$$

and

$$\tfrac{1}{2}(\epsilon_1 - \epsilon_2) = s^{1/2}/\sqrt{3} + O(s^{-1/2}). \tag{A 11}$$

In view of (A 3)–(A 5), (A 10) and (A 11), for $p \to 0$ ($s \to \infty$) the asymptotics are

$$(1+\lambda_1)^{1/2} = (1/s + O(s^{-3/2}))^{1/2} = s^{-1/2} + O(1/s) \tag{A 12}$$

and

$$(1+\lambda_2)^{1/2} = \left(\mathrm{i}s^{1/2} + \frac{3}{2} + O(s^{-1/2})\right)^{1/2} = \frac{1+\mathrm{i}}{\sqrt{2}}s^{1/4}\left(1 + \frac{3}{2\mathrm{i}}s^{-1/2} + O\left(\frac{1}{s}\right)\right)^{1/2}$$

$$= \frac{1+\mathrm{i}}{\sqrt{2}}s^{1/4} + \frac{3(1-\mathrm{i})}{4\sqrt{2}}s^{-1/4} + O(s^{-3/4}). \tag{A 13}$$

Now, in view of (A 2) and (A 12), the absolute values of exponents in (21) can be estimated:

$$Re((1+\lambda_i)^{1/2}pH) = (2Ta)^{1/2}Hs^{-1/4}Re(1+\lambda_i)^{1/2} = (Ta)^{1/2}H\,Re((1+\lambda_i)^{1/2})\frac{p}{Ta^{1/2}}, \tag{A 14}$$

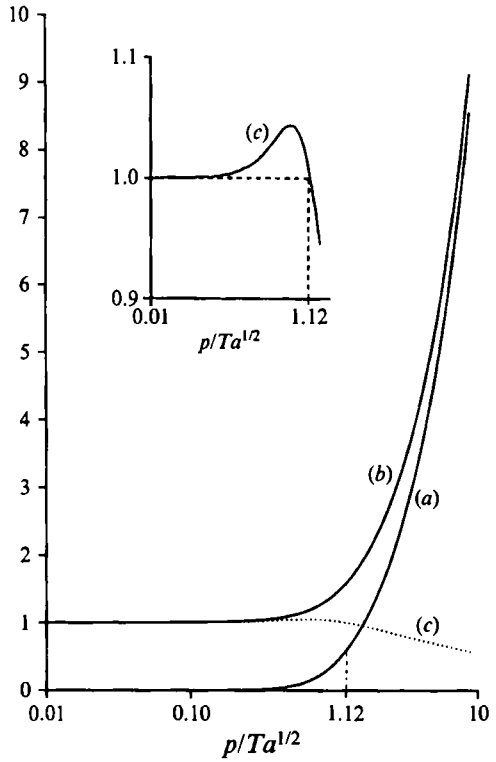

FIGURE 9. The functions (*a*) $(1+\lambda_1)^{1/2}(p/Ta^{1/2})$, (*b*) $Re\{(1+\lambda_2)^{1/2}(p/Ta^{1/2})\}$ and (*c*) the difference (*b*) − (*a*) *vs.* $p/Ta^{1/2}$ (with a portion of (*c*) enlarged). Recall that $p/Ta^{1/2} = \sqrt{2}s^{-1/4}$.

i.e. they are functions of s or $p/Ta^{1/2}$ only and

$$(1+\lambda_1)^{1/2}pH = Ta^{1/2}H(\sqrt{2}s^{-3/4}+O(s^{-5/4})); \tag{A 15}$$

since λ_2 and λ_3 are complex conjugate, on the basis of (A 13)

$$Re((1+\lambda_2)^{1/2}pH) = Re((1+\lambda_3)^{1/2}pH) = Ta^{1/2}H(1+\tfrac{3}{4}s^{-1/2}+O(1/s)). \tag{A 16}$$

It is easily seen from the two last equations that

$$\lim_{p\to 0}((1+\lambda_1)^{1/2}pH) = 0, \tag{A 17}$$

$$\lim_{p\to 0} Re((1+\lambda_2)^{1/2}pH) = Ta^{1/2}H \quad \text{and} \quad Re((1+\lambda_2)^{1/2}pH) \geqslant Ta^{1/2}H \quad \text{for} \quad \frac{p}{Ta^{1/2}} \ll 1. \tag{A 18}$$

As indicated by numerical calculations represented in figure 9, the last inequality can be extended for arbitrary value of p:

$$Re((1+\lambda_2)^{1/2}pH) = Re((1+\lambda_3)^{1/2}pH) = Ta^{1/2}H\,Re((1+\lambda_2)^{1/2})\frac{p}{Ta^{1/2}} \geqslant Ta^{1/2}H. \tag{A 19}$$

Additional useful numerical outcomes are

$$(1+\lambda_1)^{1/2}pH \geqslant \tfrac{1}{2}Ta^{1/2}H \quad \text{if} \quad p/Ta^{1/2} \geqslant 1.12, \tag{A 20}$$

$$Re((1+\lambda_2)^{1/2}pH)-(1+\lambda_1)^{1/2}pH \geqslant Ta^{1/2}H \quad \text{if} \quad p/Ta^{1/2} \leqslant 1.12. \tag{A 21}$$

Next, in view of (A 19), we obtain the following estimates, for any $p \geqslant 0$:

$$Re(\mathrm{e}^{p(1+\lambda_2)^{1/2}H}) \geqslant \mathrm{e}^{Ta^{1/2}H}, \tag{A 22a}$$

$$\sinh(p(1+\lambda_2)^{1/2}H) = \tfrac{1}{2}\mathrm{e}^{p(1+\lambda_2)^{1/2}H}(1-\mathrm{e}^{-2p(1+\lambda_2)^{1/2}H}) = \tfrac{1}{2}\mathrm{e}^{p(1+\lambda_2)^{1/2}H}(1+O(\mathrm{e}^{-2Ta^{1/2}H})) \tag{A 22b}$$

$$\cosh(p(1+\lambda_2)^{1/2}H) = \tfrac{1}{2}\mathrm{e}^{p(1+\lambda_2)^{1/2}H}(1+\mathrm{e}^{-2p(1+\lambda_2)^{1/2}H}) = \tfrac{1}{2}\mathrm{e}^{p(1+\lambda_2)^{1/2}H}(1+O(\mathrm{e}^{-2Ta^{1/2}H})). \tag{A 22c}$$

Results (A 22) are also valid when the subscript 2 is replaced by 3.

In view of (A 20)–(A 21)

$$\sinh(p(1+\lambda_1)^{1/2}H) \approx \cosh(p(1+\lambda_1)^{1/2}H) = \tfrac{1}{2}\mathrm{e}^{p(1+\lambda_1)^{1/2}H}(1+O(\mathrm{e}^{-Ta^{1/2}H})), \tag{A 23a}$$

$$\mathrm{e}^{p(1+\lambda_1)^{1/2}H} \geqslant \mathrm{e}^{1/2Ta^{1/2}H} \quad \text{if} \quad p/Ta^{1/2} \geqslant 1.12; \tag{A 23b}$$

$$\mathrm{e}^{p(1+\lambda_1)^{1/2}H} \leqslant \mathrm{e}^{p(1+\lambda_2)^{1/2}H}\mathrm{e}^{-Ta^{1/2}H} \quad \text{if} \quad p/Ta^{1/2} \leqslant 1.12; \tag{A 23c}$$

In the limit $p \to \infty$, in view of (A 2)–(A 7), $\lambda_i \to 0$ and for $i = 1, 2, 3$ we get

$$Re((1+\lambda_i)^{1/2}pH) = pH(1+o(1)). \tag{A 24}$$

In the range of $p/Ta^{1/2} \gg 1$ (A 22) and (A 23) can be strengthened, namely

$$\sinh(p(1+\lambda_i)^{1/2}H) \approx \cosh(p(1+\lambda_i)^{1/2}H) = \tfrac{1}{2}\mathrm{e}^{p(1+\lambda_i)^{1/2}H}(1+O(\mathrm{e}^{-pH})). \tag{A 25}$$

The proof of (22)–(24) is based on the preceding estimates. The details may be obtained from the authors or JFM editorial office.

Appendix B. Some approximate results for short containers

B.1. The slightly viscous 'quasi-geostrophic' core

The geostrophic core approximation discards the mass transport in the region $0^+ < z < H^-$ outside the Ekman layers; the purpose here is to incorporate this effect, which is essential in the 'outer' ($\frac{1}{4}$) Stewartson layer at least. As remarked in Moore & Saffman (1969, §7), the 'inviscid' geostrophic core and the 'outer' ($\frac{1}{4}$) Stewartson layer can be efficiently treated without *a priori* asymptotic separation into two regions. In this combined region, to leading order in $Ta^{-1/2}$ the variables u, v, P are z-independent, and the governing equations are

$$-2Tav^c = -\mathrm{d}P^c/\mathrm{d}r, \tag{B 1}$$

$$2Tau^c = \frac{\mathrm{d}}{\mathrm{d}r}\frac{1}{r}\frac{\mathrm{d}}{\mathrm{d}r}rv^c, \tag{B 2}$$

$$0 = -\partial P^c/\partial z, \tag{B 3}$$

$$\frac{1}{r}\frac{\mathrm{d}}{\mathrm{d}r}ru^c + \frac{\partial w^c}{\partial z} = 0, \tag{B 4}$$

where the superscript c means 'core'. The behaviour of the term on the right-hand side in the azimuthal momentum balance (B 2) is of interest: when it vanishes (or is discarded) the inviscid geostrophic balance is recovered by the system (B 1)–(B 4). We also note that by simplifying this term to $\mathrm{d}^2v/\mathrm{d}r^2$ we obtain the $\frac{1}{4}$ boundary layer equations.

We assume that the $\frac{1}{3}$ layer is very thin.

The above-mentioned core is matched to the boundaries by Ekman layers. The Ekman layer carries the volume flux

$$\tilde{Q}^b = Ta^{-1/2}\int_0^\infty \tilde{u}\,\mathrm{d}\zeta = -\tfrac{1}{2}Ta^{-1/2}(v^c - v^b), \tag{B 5}$$

where $\tilde{u}$ is the radial velocity correction in the layer, ζ is the local distance stretched by $Ta^{1/2}$, and the superscript b denotes the appropriate boundary (top, bottom or disk); here $v^b = 0$.

A single equation for v^c can be obtained as follows. First, we note that global continuity in a cylindrical control volume of radius $r\,(<1)$, from disk to top wall, reads

$$2\pi r[u^c H + \tilde{Q}^{disk} + \tilde{Q}^{top}] = \pi r^2 \tag{B 6}$$

where the right-hand side expresses the rate of volume reduction due to the axial motion of the disk. Next, by substituting (B 2) and (B 5) we obtain

$$\epsilon^2\left(\frac{\mathrm{d}^2v}{\mathrm{d}r^2} + \frac{1}{r}\frac{\mathrm{d}v}{\mathrm{d}r} - \frac{v}{r^2}\right) - v = \frac{1}{2}Ta^{1/2}r, \tag{B 7}$$

where

$$\epsilon = (\tfrac{1}{2}H\,Ta^{-1/2})^{1/2}, \tag{B 8}$$

and subject to the boundary condition

$$\frac{\mathrm{d}v}{\mathrm{d}r}(r=0) = v(r=1) = 0; \tag{B 9}$$

hereafter the superscript c is dropped.

The solution is

$$v = -\tfrac{1}{2}rTa^{1/2}\left[1 - \frac{I_1(r/\epsilon)}{rI_1(1/\epsilon)}\right]. \tag{B 10}$$

In the downstream region $z < 0$ the same v but with opposite sign prevails.

In view of (52), (B 1) and (B 10), the drag on the disk is

$$D = -2\pi Ta\int_0^1 (v^T - v^B)\,r^2\,\mathrm{d}r = -2\pi Ta\int_0^1 2vr^2\,\mathrm{d}r = \frac{\pi}{2}Ta^{3/2}\left[1 - 4\epsilon\frac{I_2(1/\epsilon)}{I_1(1/\epsilon)}\right]. \tag{B 11}$$

For $\epsilon \ll 1$ the leading asymptotic terms in (B 10), (B 11) give

$$v = -\tfrac{1}{2}rTa^{1/2}\left[1 - \exp\left(\frac{r-1}{\epsilon}\right)\right] \quad \text{for} \quad r \gg \epsilon; \tag{B 12}$$

$$D = \tfrac{1}{2}\pi\,Ta^{3/2}[1 - 4\epsilon(1 - \tfrac{3}{2}\epsilon)]. \tag{B 13}$$

Evidently, for $\epsilon \to 0$ the 'inviscid' geostrophic core results, $v = \frac{1}{2}rTa^{1/2}$ and $D_0 = \frac{1}{2}\pi\,Ta^{3/2}$, are recovered, and the $\frac{1}{4}$ layer near $r = 1$ is seen in (B 12).

Result (B 11), although indicative, is less useful than anticipated: comparisons with the exact solution indicate that the quasi-geostrophic correction to D_0 is not accurate

Ta	H	ϵ	D/D_0, exact	D/D_0, (B 11)	$\delta^{1/3}/\epsilon$	$\delta^{1/3}$
10^3	1	0.126	0.91	0.59	0.8	0.10
	5	0.282	0.62	0.34	0.6	0.17
	8	0.356	0.53	0.22	0.6	0.20
10^4	0.5	0.050	0.94	0.81	0.8	0.04
	1	0.071	0.89	0.75	0.7	0.05
	5	0.158	0.69	0.51	0.5	0.08
	8	0.200	0.61	0.43	0.5	0.09
	15	0.274	0.49	0.31	0.4	0.11
	50	0.500	0.27	0.13	0.3	0.17
	100	0.707	0.18	0.07	0.3	0.22
$2.6\,10^4$	0.5	0.039	0.92	0.85	0.7	0.03
	1	0.056	0.88	0.80	0.6	0.03
	2	0.079	0.82	0.72	0.5	0.04
	3	0.096	0.78	0.67	0.5	0.05
	4	0.111	0.75	0.63	0.5	0.05
	5	0.125	0.72	0.59	0.5	0.06
	8	0.158	0.65	0.51	0.4	0.07
	10	0.176	0.61	0.47	0.4	0.07
	15	0.216	0.54	0.40	0.4	0.08

TABLE 1. Influence of ϵ and other parameters on the drag: $\delta^{1/3} = (H/Ta)^{1/3}$ estimates the thickness of the inner Stewartson layer; $\epsilon/\delta^{1/3}$ estimates the ratio of the thickness of the outer and inner Stewartson layers.

in many cases of interest, see table 1. Indeed, the asymptotic model implies the quite obvious requirement that the inner $\frac{1}{3}$ layer should be much thinner than the outer Stewartson layer, i.e. $\delta^{1/3}/\epsilon \approx (H^2 Ta)^{-1/12} \ll 1$. Otherwise the $\frac{1}{3}$-layer pressure correction near the rim may influence the drag by an amount commensurate with the contribution of the $\frac{1}{4}$ layer. In the range under investigation, and actually for any practically attainable configuration, $(H^2 Ta)^{-1/12}$ is not small. This is illustrated in table 1: it turns out that the ratio $\delta^{1/3}/\epsilon$ is not small and/or the $\frac{1}{3}$ layer is quite thick for all the tested combinations of Ta, H. These results also indicate that the range of parameters covered by the 'short container' asymptotic model is practically unattainable.

The radial velocity in the upper region is readily obtained from (B 6), upon substituting (B 5) and (B 10), as

$$u = \frac{1}{2H} \frac{I_1(r/\epsilon)}{I_1(1/\epsilon)}. \tag{B 14}$$

Equation (B 7) shows that the ratio of $-v$ to the term on the right-hand side gives the relative amount of mass transported by the Ekman layers. For $\epsilon = 1$ this ratio equals 0.12, 0.09, 0.04 at $r = 0.01, 0.5, 0.8$, respectively; for larger ϵ the corresponding ratios are about ϵ^2 times smaller.

B.2. *Disk in off-middle position*

Let the distances of the disk from the top and bottom walls be H_T and H_B, respectively, with $H_T + H_B = 2H$, and the index O denote the outer region, $r > 1$, see figure 1.

The asymmetry $H_T \neq H_B$ with respect to z causes different thicknesses of the vertical shear regions, and rotation ω^{disk} of the disk. We attempt to estimate the influence of these effects on the drag; for small values of ϵ we anticipate

$$D \approx D_0[1 - 4\epsilon\phi(\mathscr{R})], \tag{B 15}$$

cf. (B 13), where

$$\mathscr{R} = H_T/H_B \quad \text{and} \quad \phi(1) = 1. \tag{B 16}$$

Following (B 8) we define

$$\epsilon_T = (H_T/H)^{1/2}\epsilon; \quad \epsilon_B = (H_B/H)^{1/2}\epsilon; \quad \epsilon_O = \sqrt{2}\epsilon. \tag{B 17}$$

For simplicity of analysis we assume that $\epsilon \ll 1$, hence the vertical shear layers at top, bottom and outer side of the disk are thin. The swirl velocities are expected to be

$$\omega^T(r) = \omega_0^T[1 - A_T \exp((-1+r)/\epsilon_T)], \tag{B 18}$$

$$\omega^B(r) = \omega_0^B[1 - A_B \exp((-1+r)/\epsilon_B)], \tag{B 19}$$

$$\omega^O(r) = B\exp((1-r)/\epsilon_O), \tag{B 20}$$

where ω_0^T, ω_0^B, A_T, A_B, B are constants. This flow field must satisfy: (*a*) global volume transport requirements; (*b*) the condition of zero torque on disk, and (*c*) the matching conditions (Moore & Saffman 1969):

$$\omega^T(r=1) = \omega^B(r=1) = \omega^O(r=1); \tag{B 21}$$

$$(\mathrm{d}/\mathrm{d}r)[H_T\omega^T(r) + H_B\omega^B(r) - 2H\omega^O(r)] = 0. \tag{B 22}$$

In the inviscid core region the volume transport is performed by the Ekman layers. In view of (B 5), (B 18), and (B 19) this is expressed as

$$2\pi r^2[-\tfrac{1}{2}Ta^{-1/2}(\omega_0^T - \omega^{disk}) - \tfrac{1}{2}Ta^{-1/2}\omega_0^T] = \pi r^2; \tag{B 23}$$

$$2\pi r^2[-\tfrac{1}{2}Ta^{-1/2}(\omega_0^B - \omega^{disk}) - \tfrac{1}{2}Ta^{-1/2}\omega_0^B] = -\pi r^2. \tag{B 24}$$

This readily gives

$$\omega^{disk} = \omega_0^T + \omega_0^B, \tag{B 25}$$

$$\omega_0^T = -\tfrac{1}{2}Ta^{-1/2} + \tfrac{1}{2}\omega^{disk}; \quad \omega_0^B = \tfrac{1}{2}Ta^{-1/2} + \tfrac{1}{2}\omega^{disk}. \tag{B 26}$$

The torque on the disk comes from the shear in the Ekman layer, e.g. $\tau_{\theta z}^T = Ta^{-1/2}r(\omega^T - \omega^{disk})$. Integrating $(2\pi r^2\,\mathrm{d}r)\tau_{\theta z}$ from 0 to 1 on both sides of the disk we obtain, approximately, the torque-free disk condition as

$$\tfrac{1}{4}(\omega_0^T + \omega_0^B - 2\omega^{disk}) - (\omega_0^T A_T \epsilon_T + \omega_0^B A_B \epsilon_B) = 0. \tag{B 27}$$

In view of (B 25) we get

$$\omega^{disk} = -4(\omega_0^T A_T \epsilon_T + \omega_0^B A_B \epsilon_B); \tag{B 28}$$

since A_T, A_B are $O(1)$, $\omega^{disk} = O(\epsilon Ta^{1/2}) = O(Ta^{1/4})$.

Substituting (B 26) and (B 18)–(B 20) in (B 21)–(B 22) and taking into account (B 28) yields, to leading order in ϵ,

$$A_T = \frac{(1+\mathscr{R})^{1/2}+2}{(1+\mathscr{R})^{1/2}+\mathscr{R}^{1/2}+1}; \quad A_B = 2 - A_T. \tag{B 29}$$

Now we proceed to the calculation of the drag, see (B 11),

$$\begin{aligned} D &= -2\pi Ta\int_0^1 [\omega^T(r) - \omega^B(r)]\, r^3\,\mathrm{d}r \\ &= -2\pi Ta\int_0^1 (\omega_0^T - \omega_0^B)\, r^3\,\mathrm{d}r \\ &\quad -2\pi Ta\int_0^1 \left[-\omega_0^T A_T \exp\left(\frac{-1+r}{\epsilon_T}\right) + \omega_0^B A_B \exp\left(\frac{-1+r}{\epsilon_B}\right)\right] r^3\,\mathrm{d}r \\ &\approx D_0 - 2\pi Ta^{3/2}(\epsilon_T A_T + \epsilon_B A_B) \\ &= D_0 - 2\pi Ta^{3/2}\epsilon\phi(\mathscr{R}) = D_0[1 - 4\epsilon\phi(\mathscr{R})]; \end{aligned}$$

where

$$\phi(\mathscr{R}) = \left(\frac{2}{1+\mathscr{R}}\right)^{1/2}\left[1+\tfrac{1}{2}(\mathscr{R}^{1/2}-1)\frac{(1+\mathscr{R})^{1/2}+2}{(1+\mathscr{R})^{1/2}+\mathscr{R}^{1/2}+1}\right]. \tag{B 30}$$

As expected, $\phi(\mathscr{R}) = \phi(1/\mathscr{R})$. The maximum of $\phi(\mathscr{R})$ is 1 at $\mathscr{R} = 1$ and the minimum is $\sqrt{2}/4$ at $\mathscr{R} = 0$ and $\mathscr{R} \to \infty$; for $0.5 < \mathscr{R} < 2$ the values of $\phi(\mathscr{R})$ deviate from 1 by at most 3.2%.

REFERENCES

ABRAMOWITZ, M. & STEGUN, I. A. 1964 *Handbook of Mathematical Functions*. Dover.

BARNARD, B. J. S. & PRITCHARD, W. G. 1975 The motion generated by a body moving through a stratified fluid at large Richardson numbers. *J. Fluid Mech.* **71**, 43–64.

GREENSPAN, H. P. 1968 *The Theory of Rotating Fluids*. Cambridge University Press.

HOCKING, L. M., MOORE, D. W. & WALTON, I. C. 1979 The drag on a sphere moving axially in a long rotating container. *J. Fluid Mech.* **90**, 781–793.

KANTOROVICH, L. V. & KRYLOV, V. I. 1964 *Approximate Methods of Higher Analysis*. Interscience.

MAXWORTHY, T. 1968 The observed motion of a sphere through a short, rotating cylinder of fluid. *J. Fluid Mech.* **31**, 643–655.

MAXWORTHY, T. 1970 The flow created by a sphere moving along the axis of a rotating, slightly-viscous fluid. *J. Fluid Mech.* **40**, 453–479.

MOORE, D. W. & SAFFMAN, P. G. 1968 The rise of a body through a rotating fluid in a container of finite length. *J. Fluid Mech.* **31**, 635–642.

MOORE, D. W. & SAFFMAN, P. G. 1969 The structure of free vertical shear layers in a rotating fluid and the motion produced by a slowly rising body. *Phil. Trans. R. Soc. Lond.* A **264**, 597–634.

RAY, M. 1936 Application of Bessel functions in the solution of problems of motion of a circular disk in viscous liquid. *Phil. Mag.* (7) **21**, 546–564.

STEWARTSON, K. 1952 On the slow motion of an ellipsoid in a rotating fluid. *Q. J. Mech. Appl. Maths* **6**, 141–162.

TANZOSH, J. & STONE, H. A. 1994 Motion of a rigid particle in a rotating viscous flow: an integral equation approach. *J. Fluid Mech.* **275**, 225–256.

TRANTER, C. J. 1951 *Integral Transforms in Mathematical Physics*. Methuen.

UNGARISH, M. 1993 *Hydrodynamics of Suspensions*. Springer, Berlin.

UNGARISH, M. 1995 Some shear-layer and inertial modifications of the geostrophic drag on a slowly rising particle or drop in a rotating fluid, in preparation.

VEDENSKY, D. & UNGARISH, M. 1994 The motion generated by a slowly rising disk in an unbounded rotating fluid for arbitrary Taylor number. *J. Fluid Mech.* **262**, 1–26 (referred to herein as VU).

WATSON, G. N. 1952 *A Treatise on the Theory of Bessel Functions*. Cambridge University Press.

WEISENBORN, A. J. 1985 Drag on a sphere moving slowly in a rotating viscous fluid. *J. Fluid Mech.* **153**, 215–227.